

# Uniform postglacial slip-rate along the central 600 km of the Kunlun Fault (Tibet), from $^{26}\text{Al}$ , $^{10}\text{Be}$ , and $^{14}\text{C}$ dating of riser offsets, and climatic origin of the regional morphology

Jerome Van Der Woerd,<sup>1,2\*</sup> Paul Tapponnier,<sup>1</sup> Frederick J. Ryerson,<sup>2</sup> Anne-Sophie Meriaux,<sup>1,2</sup> Bertrand Meyer,<sup>1</sup> Yves Gaudemer,<sup>1</sup> Robert C. Finkel,<sup>2</sup> Marc W. Caffee,<sup>2</sup> Zhao Guanguang<sup>3</sup> and Xu Zhiqin<sup>4</sup>

<sup>1</sup>Institut de Physique du Globe de Paris, 4 Place Jussieu, 75252 Paris Cedex 05, France

<sup>2</sup>Institute of Geophysics and Planetary Physics, Lawrence Livermore National Laboratory, Livermore, CA 94550, USA.

<sup>3</sup>Institute of Crustal Dynamic, State Seismological Bureau, Beijing 100085, People's Republic of China

<sup>4</sup>Institute of Geology, Chinese Academy of Geological Sciences, 26 Baiwanzhuang Road, Beijing 100037, People's Republic of China

Accepted 2001 June 29. Received 2001 February 26; in original form 2000 January 16

## SUMMARY

Late Pleistocene–Holocene sinistral slip-rates on several segments of the Kunlun Fault in northeastern Tibet have been determined. These determinations are based on the measured displacement of alluvial surfaces whose surface ages were determined by cosmogenic  $^{26}\text{Al}$  and  $^{10}\text{Be}$  dating of quartz pebbles, and by  $^{14}\text{C}$  dating of charcoal. In the west, at three sites along the Xidatan–Dongdatan segment of the fault, near  $94^\circ\text{E}$ , terrace riser offsets ranging from 24 to 110 m, with cosmogenic ages ranging from  $\sim 1800$  to  $\sim 8200$  yr, yield a mean left-lateral slip-rate of  $11.7 \pm 1.5$  mm yr<sup>-1</sup>. Field observations indicate minimum offsets of 9–12 m; this offset, when combined with the long-term slip-rate, indicates that great earthquakes ( $M \sim 8$ ) rupture this segment of the fault with a recurrence interval of 800–1000 yr. At two sites along the Dongxi–Anyemaqin segment of the fault, near  $99^\circ\text{E}$ , terrace riser offsets ranging from 57 to 400 m with  $^{14}\text{C}$  ages ranging from 5400 to 37 000 yr BP yield a minimum slip-rate of  $\sim 10$  mm yr<sup>-1</sup>. At one site, the 1937 January 7,  $M=7.5$  and the penultimate earthquakes produced 4 m of left-slip and 0.4 m of reverse-slip. The maximum recurrence interval of earthquakes with such characteristic slip is thus  $\sim 400$  yr. Farther east, near  $100.5^\circ\text{E}$ , along the Maqen segment of the fault, the 180 m offset of a lateral moraine, emplaced between the last glacial maximum (20 ka) and 11 100 yr BP, yields a mean slip-rate of  $12.5 \pm 2.5$  mm yr<sup>-1</sup>.

The slip-rates are constant, within uncertainty, throughout the 600 km of the Kunlun Fault that we studied. The average slip-rate is  $11.5 \pm 2.0$  mm yr<sup>-1</sup>. Extrapolating this rate to the remainder of the fault, we conclude that most (80 per cent) of the 300 morphological offsets measured in the field or on SPOT satellite images post-date the Last Glacial Maximum. Most of the terraces we studied were deposited during the humid period of the Early Holocene Optimum (9–5 ka); the formation of younger terraces reflects Late Holocene climate change.

**Key words:**  $^{26}\text{Al}$ ,  $^{10}\text{Be}$  and  $^{14}\text{C}$  dating, faulting, geomorphology, Kunlun Fault, palaeoclimate, Tibet.

## 1 INTRODUCTION

The Kunlun, Altyn Tagh, and Haiyuan strike-slip faults bound the northern Tibetan Plateau (Fig. 1) (e.g. Tapponnier & Molnar 1977; Tapponnier *et al.* 1982; Deng *et al.* 1986;

Peltzer & Tapponnier 1988a; England & Molnar 1990; Avouac & Tapponnier 1993). Their great lateral extent and spatial relationship to high-angle shortening features—large thrusts and growing mountain ranges—suggest that they play a major role in accommodating Indo-Asian convergence (e.g. Tapponnier *et al.* 1990; Meyer *et al.* 1998). An accurate knowledge of the slip-rates along these faults of northern Tibet is essential to assess the large-scale mechanical behaviour of the crust and mantle beneath

\* Now at: Equipe de Tectonique, EOST-IPG5, 5, rue R. Descartes, 67084 Strasbourg Cedex.

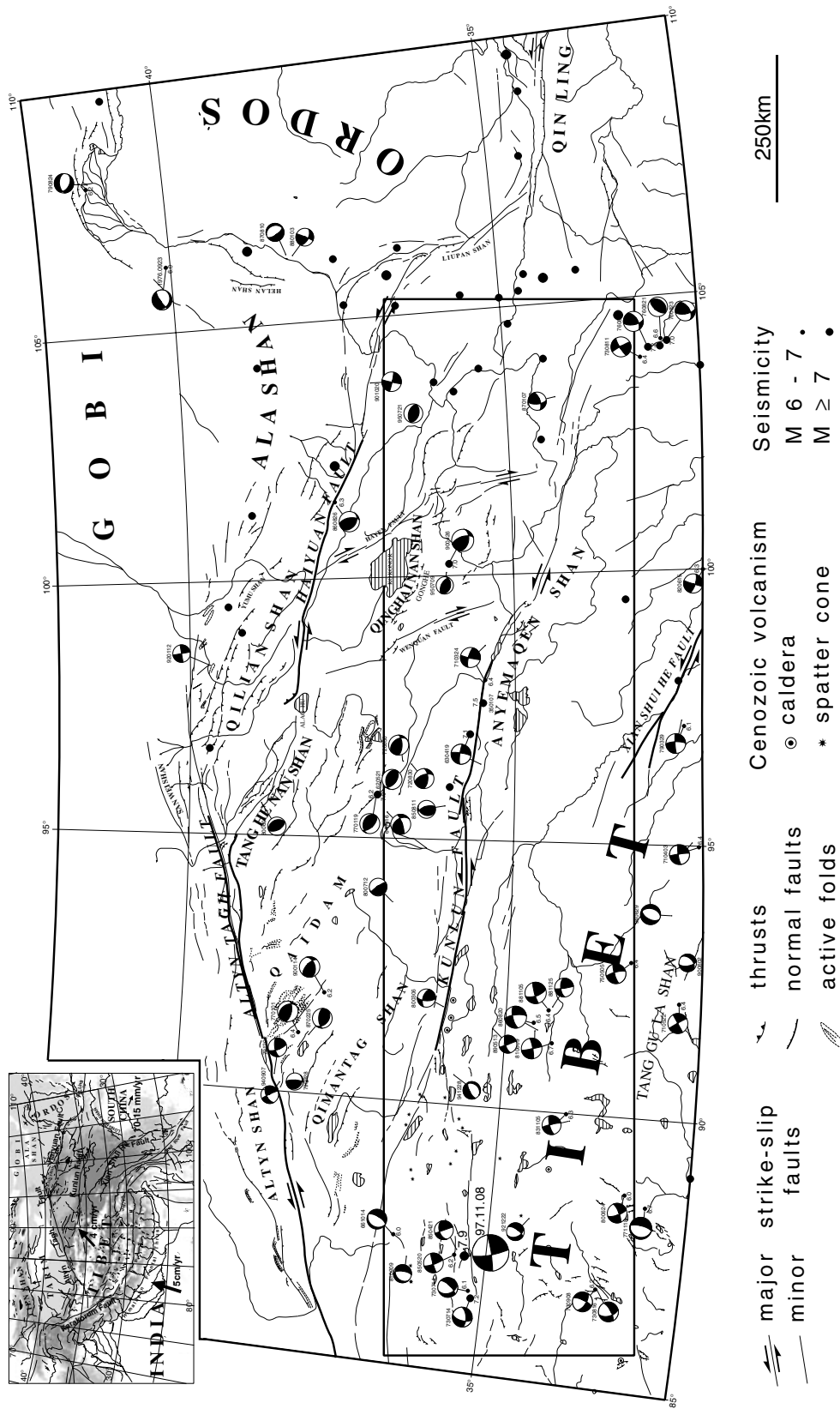


**Figure 1.** Seismotectonic map of northern Tibet. Inset shows the location of the map within the India-Asia collision framework. Northern Tibet is bounded by three major left-lateral strike-slip faults: the Altn Tagh, Kunlun and Haiyuan faults. The Kunlun Fault extends from 86°E to 105°E over 1500 km and separates the high plateau to the south from the northwestern margin of Tibet. East of 91°E it can be traced almost continuously along disrupted and faulted piedmont. The western termination of the Kunlun Fault splays into several fault strands; the northern one probably merges with the Altn Tagh Fault; the southwesternmost one ruptured during the  $M_s = 7.9$ , 1997 November 8 Manyi left-lateral earthquake (Peltzer *et al.* 1999; Velasco *et al.* 2000). Seismicity is from instrumental (USGS 1977-1998) and historical (Gu *et al.* 1989) catalogues. Focal mechanisms are from Molnar & Lyon-Caen (1989) and USGS. Box is the location of Fig. 2.

**Table 1** Summary of large earthquakes of north Tibet on large strike-slip faults or nearby thrusts.

| Name     | Date       | Magnitude | Fault             | $\Delta u$ , L      | References  |
|----------|------------|-----------|-------------------|---------------------|---|
| Haiyuan  | 12.20.1920 | 8.7       | Haiyuan Fault     | 8 m, 220 km         | Deng <i>et al.</i> 1986; Zhang <i>et al.</i> 1987       |
| Gulang   | 05.23.1927 | 8.3       | Dongqiding thrust | 1.5–4 m, ~60 km     | Deng <i>et al.</i> 1984; Gaudemer <i>et al.</i> 1995b   |
| Minfeng  | 07.03.1924 | 7.2       | Altyn Tagh Fault  | (? / 45–140 km)     | Molnar and Deng 1984; Ge 1992                           |
| Minfeng  | 07.11.1924 | 7.2       | Altyn Tagh Fault  | (? / 45–140 km)     | Molnar and Deng 1984; Ge 1992                           |
| Chang Ma | 12.25.1932 | 7.6       | Chang Ma Fault    | 6.2 m, 150 km       | Meyer 1991; Peltzer <i>et al.</i> 1988a                 |
| Tuosuohu | 01.01.1937 | 7.5       | Kunlun Fault      | 4.4–7 m, >150 km    | Tapponnier and Molnar 1977; Li and Jia 1981             |
| Tuosuohu | 04.19.1963 | 7.1       | Kunlun Fault      | (2.3–8 m, 150 km ?) | Tapponnier and Molnar 1977; Li and Jia 1981             |
| –        | 03.24.1971 | 6.4       | Kunlun Fault      | –                   | Tapponnier and Molnar 1977                              |
| Manyi    | 11.08.1997 | 7.9 (Ms)  | Kunlun Fault      | 7 m, 150 km         | Peltzer <i>et al.</i> 1999; Velasco <i>et al.</i> 2000. |

the plateau, and to test the predictions of various controversial models (e.g. England & Houseman 1986; Avouac & Tapponnier 1993; England & Molnar 1997; Meyer *et al.* 1998).

The largest earthquakes recorded this century in northern Tibet (Gu *et al.* 1989) ruptured segments of these sinistral faults or nearby thrusts (Table 1). In particular, three large earthquakes (1937 January 7, 1963 April 19, and 1971 March 24), with magnitudes of 7.5, 7.1 and 6.4, respectively (Fig. 2) (e.g. Tapponnier & Molnar 1977; Cui & Yang 1979; Molnar & Deng 1984; Gu *et al.* 1989) ruptured the central stretch of the Kunlun Fault. Together, the 1963 and 1937 surface breaks were reported to reach a cumulative length of about 300 km, with maximum horizontal displacements of 7–8 m (e.g. Li & Jia 1981; Molnar & Lyon-Caen 1989). More recently, on 1997 November 8, the largest earthquake ( $M_s = 7.9$ ) ever recorded instrumentally in northern Tibet (Peltzer *et al.* 1999; Velasco *et al.* 2000) appears to have ruptured one of the westernmost, N80°E-striking segments of the Kunlun Fault, between 86°E and 90°E, a feature

previously mapped on Landsat images by Tapponnier & Molnar (1977; Fig. 2). The rupture length was in excess of 150 km, and the maximum horizontal slip was ~7 m (Peltzer *et al.* 1999). The sizes and recurrence intervals of large palaeoearthquakes on the Kunlun Fault are unknown, however. Similarly, its slip-rate remains poorly constrained. The Quaternary average slip-rate at the Kunlun Pass (Fig. 2) has long been estimated to be between 10 and 20 mm yr<sup>-1</sup> (Kidd & Molnar 1988). Recent GPS results, based on the displacements of a small number of monuments far from the fault, however, suggest a much smaller rate, of the order of only 6 mm yr<sup>-1</sup> (Chen *et al.* 2000). In a preliminary study in which we pioneered the use of cosmogenic exposure dating to determine the ages of terrace risers offset by the fault, we obtained, at one site east of the Kunlun Pass (site 1, Fig. 2), a Late Holocene mean slip-rate of  $12 \pm 2.6$  mm yr<sup>-1</sup> (Van Der Woerd *et al.* 1998), consistent with that (11.5 mm yr<sup>-1</sup>) inferred by Zhao (1996) from <sup>14</sup>C dating of other offsets in the same area.

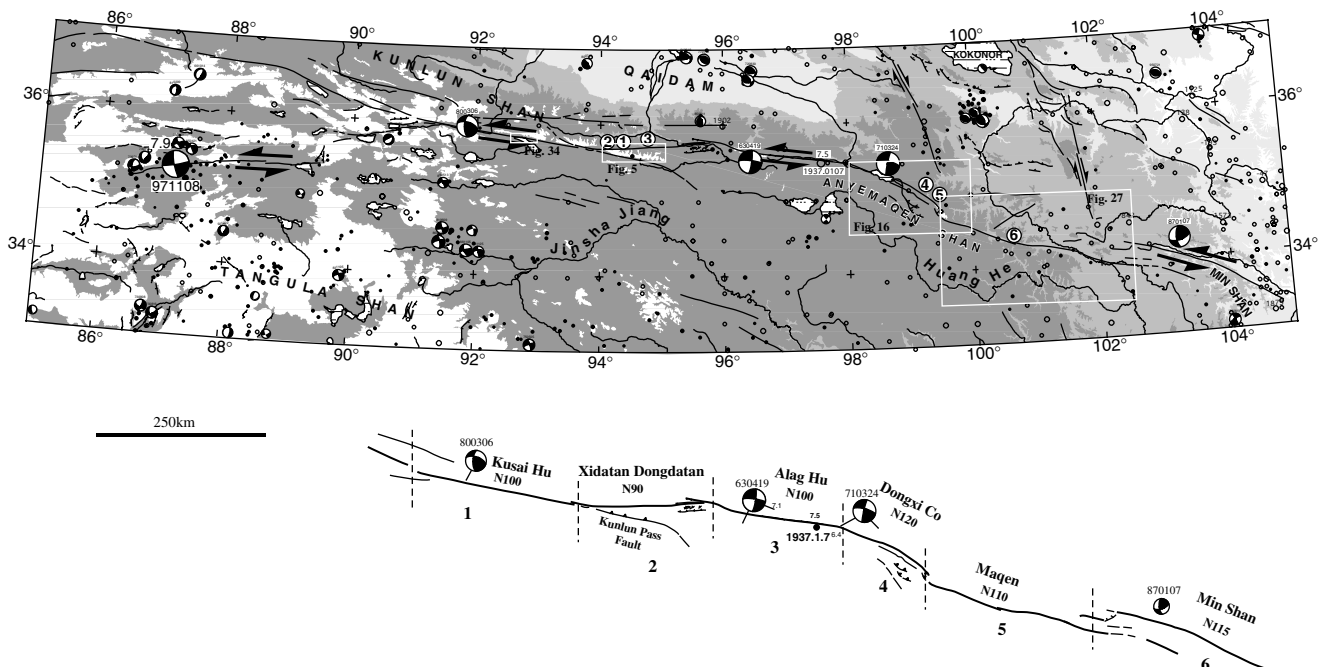


**Figure 2.** Large-scale segmentation of Kunlun Fault. From 91°E to 105°E, six segments are identified. Min Shan segment (103°E to 105°E) steps about 50 km to the north. West of 91°E, several segments, with strikes between N70°E and N140°E, linked with normal faults form the broad western horsetail termination. Instrumental (USGS 1977–1998) and historical (Gu *et al.* 1989) seismicity, filled and open circles, respectively, is shown for magnitude  $M_s > 4$ . Focal mechanisms are from Molnar & Lyon-Caen (1989) and USGS. White boxes refer to figures, circled numbers to sites studied in the field.

In order to quantify slip-rates and earthquake recurrence intervals on the Kunlun Fault, we studied offset surface landforms along more than a third of its length (600 km). We present here in detail the data and results of this study, recently summarized in Van der Woerd *et al.* (2000). We used SPOT satellite imagery to identify prominent cumulative offsets along-strike. Three segments of the fault that could be more easily reached were targeted for detailed fieldwork. Air photos and 1/100 000 scale topographic maps were used for precise mapping of the Quaternary geology surrounding displaced geomorphic features. In the west, at three sites along the western part of the Xidatan–Dongdatan valley, where many inset terrace risers are cut and offset different amounts by the fault-trace, cosmogenic dating of pebbles was used to constrain the terrace surface ages and assess possible slip-rate variations along-strike and with time. Near Dongxi Co and Maqen, along the central and eastern stretches of the fault, where the cosmogenic technique was less suitable, offset ages were constrained by radiocarbon dating. The rate we find is approximately constant over the time-span and fault length sampled, permitting an estimate of the ages of unsampled offset features elsewhere along the fault. The measured and inferred ages suggest that the regional morphology was shaped by climate change.

## 2 LARGE-SCALE SEGMENTATION OF THE FAULT

The 1600 km long Kunlun Fault system extends between 87°E and 105°E, from the high Qiangtang platform of northern Tibet, a dry permafrost plateau over 5000 m a.s.l., down to the humid, forested and deeply incised (2000 m a.s.l. on average)

mountainous rim of southern China's Sichuan basin (Figs 2 and 3). The intervening topography results from the competing forces of tectonic uplift and mountain building on the one hand, and glacial abrasion and fluvial incision on the other. Internal drainage and deposition within landlocked, high-altitude basins, with a cold-arid climate and glacial-periglacial environment, predominate in the west, while the mountains in the east, which enjoy a moist temperate climatic environment, are drained by large streams that reach the sea. The longitudinal climatic variation results from the combined changes of moisture supply, with monsoonal rainfalls coming from the southeast, and of elevation, which increases gradually westwards by more than 3000 m (Fig. 3; Derbyshire *et al.* 1991; Wang & Derbyshire 1987; Lehmkuhl *et al.* 1998). Extant palaeoclimatic studies of northern Tibet and adjacent regions suggest that the largest, most recent climatic change, the global warming that marked the end of the Würm glaciation, strongly affected landforms throughout the area (Gasse *et al.* 1991; Lister *et al.* 1991; Pachur *et al.* 1995; Assaraj 1997; Liu *et al.* 1998; Thompson *et al.* 1989, 1997; Lehmkuhl *et al.* 1998; Yan *et al.* 1999).

On a large scale, the Kunlun Fault system follows the northeastern border of the highest part of the Tibet Plateau, and is slightly concave towards the south. It is composed of 12 principal linear segments (Fig. 2), which can be clearly identified on Landsat and SPOT satellite images. Overall, the fault-plane solutions, the strike-perpendicular components of dip-slip, and the associated geomorphic structures (pull-aparts, restraining bends) along the entire length of the fault imply a consistent pattern of pure left-lateral strike-slip along the segments that trend N105–110°E, while those trending N80–105°E tend to display oblique normal faulting, and those trending N110–130°E display thrust components of slip.

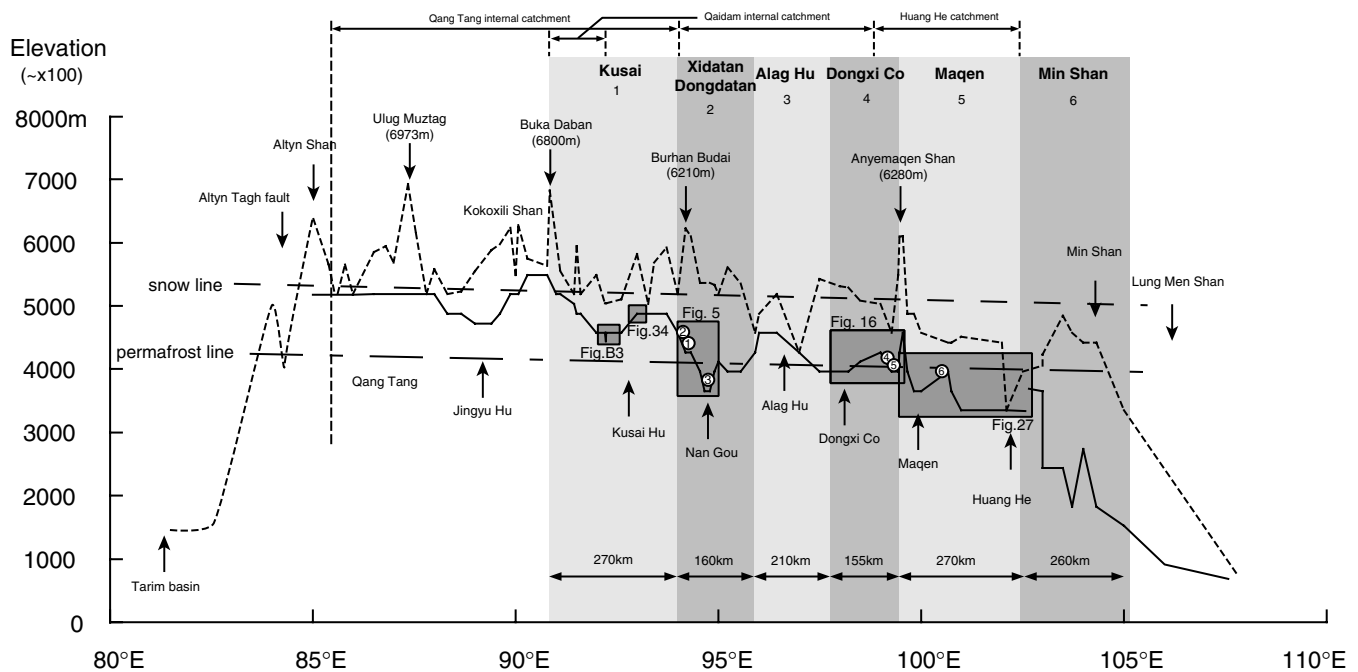


**Figure 3.** Elevation along the Kunlun Fault (continuous line) from west to east. The fault strikes roughly east–west between 34°N and 37°N. The dashed line represents the highest relief south or north of fault. Both lines are from topographic ONC maps at 1 : 1000 000 scale (DMA 1980, 1987, 1988). Large-scale segmentation with segment names and lengths are represented by alternate light and dark grey shades. Snow and permafrost lines are from Wang & Derbyshire (1987). Boxes refer to Figures, and circled numbers to sites studied in the field.

West of 91°E, within northern Qiangtang, the active trace of the fault splays into an extensional horsetail with several oblique, normal-sinistral segments whose strikes range between N70°E and N140°E (Fig. 2). Although the periglacial environment (>4800 m) makes geomorphic evidence of active faulting subtler, several identifiable strike-slip fault traces can be followed westwards to at least 87°E, the northernmost one nearly all the way to the N70°E-striking Altyn Tagh Fault (Fig. 1). The faults, a few tens to several hundred kilometres long, are marked by clear sinistral offsets on Quaternary bajadas, suggesting slip transfer from the Altyn Tagh to the Kunlun Fault across a broad zone southwest of the Qimantag (Meyer *et al.* 1998) (Figs 1 and 2). This interpretation is consistent with focal mechanisms of earthquakes in the area, which show mostly extension on NE–SW-striking planes, and left-slip on N80°E-striking planes, such as for the 1997 November 8,  $M_s=7.9$  earthquake (Peltzer *et al.* 1999; Velasco *et al.* 2000; Fig. 2).

East of the ice-capped Buka Daban peak (6800 m, 91°E; Figs 2 and 3), the main Kunlun Fault trace is sharp and continuous for almost 1200 km. We divide this part of the fault into six, 150–270 km long, first-order segments, described below, on the basis of large-scale geometrical complexities (push-ups, pull-aparts, releasing or restraining bends) and uniform mean strike in between (Fig. 2). In the field, some first-order segments are composed of shorter subsegments.

The westernmost, Kusai Hu segment strikes  $\sim$ N100°E between 91°E and 94°E for about 270 km (Fig. 2). Along the southern range front of the Eastern Kunlun Shan, slip is partitioned between a normal fault, marked by triangular facets, and a parallel strike-slip trace that cuts alluvial fans and terraces 1–2 km southwards. About 30 km east of Kusai Hu, the two faults merge into a single trace with oblique motion, unroofing a narrow footwall slab of vertically foliated, mylonitic gneisses and amphibolites, with horizontal lineation (Arnaud *et al.* 1997). Near 94°E, the fault splays again into two branches. One veers northeast, forming the Xidatan–Dongdatan segment of the fault. The other veers south to form the Kunlun Pass Fault (Kidd & Molnar 1988), which strikes N110°E for 90 km to 95°E, before bending further southeastwards for another 50 km. The Kunlun Pass Fault was inferred to have a small left-lateral slip component (Kidd & Molnar 1988), but the absence of consistent horizontal offsets on air photos and SPOT images, the strike of the fault, and the 6000 m high crest line of Burhan Budai Shan just north of it indicate that it is primarily a thrust, responsible for the uplift of that range.

The Xidatan–Dongdatan segment of the fault stretches for about 160 km east of the Kunlun Pass to 95.7°E, with an average EW strike. The dominantly strike-slip trace cuts alluvial fans and terraces, crossing the flat-floored Xidatan–Dongdatan valley from southwest to northeast. Such oblique crossing and the presence of normal scarps on either side of the valley suggest that this segment of the fault now shortcuts a former pull-apart trough that extended along the valley. East of Dongdatan, the fault follows the northern edge of another large pull-apart basin whose floor is cut by numerous NE–SW-trending normal fault scarps. The fault then veers sharply by  $\sim$ 20° towards the south.

The next segment of the fault (Halag Hu) extends about 210 km to 98°E. West of Alag Hu lake, the fault splays into two more easterly striking, predominantly strike-slip strands that are parallel for  $\sim$ 100 km. Both strands cut across the piedmont bajadas of high ranges to the north and south, bounding a 5–8 km wide pull-apart trough. They ruptured during the 1963

April 19,  $M_s=7.1$ , and 1971 March 24,  $M_s=6.4$  earthquakes (Li & Jia 1981; Fig. 2). Both focal mechanisms are consistent with sinistral slip along steep,  $\sim$ N100–105°E-trending planes (Tapponnier & Molnar 1977). Near 98°E, the fault takes another sharp,  $\sim$ 10°–20° bend towards the south.

East of this bend, the Dongxi–Anyemaqen segment of the fault strikes  $\sim$ N120–130°E to 99.5°E, for about 155 km. The fault trace, which is everywhere marked by the mole tracks of the  $M=7.5$ , 1937 earthquake, enters the rhomb-shaped,  $\sim$ 40 km long, 10 km wide, Dongxi Co pull-apart lake at its southwest corner, and steps out of it at its northeast corner. That the same earthquake rupture crosses a large pull-apart lake is reminiscent of the surface break of the 1951,  $M=8$ , Damxung earthquake in south Tibet, which was mapped on either side of Beng Co Lake by Armijo *et al.* (1989). The fault trace then continues to the north slope of Anyemaqen Shan (6280 m), a fast-rising mountain range in a restraining bend of the fault (Gaudemer *et al.* 1995a; Van Der Woerd 1998). A secondary fault, south of and parallel to the main active fault trace, bounds the south slope of that range. This fault probably reflects an earlier stage of development of the Anyemaqen bend, prior to the north-directed step that led to foundering of the Dongxi Co pull-apart. Southwest of the Anyemaqen range, we mapped several active thrust faults in the field (Fig. 2), with clear evidence of postglacial throw.

East of the Anyemaqen range, the Maqen segment of the fault bends back to a N110°E strike for  $\sim$ 270 km, from 99.5°E to 102.1°E. Fluvial incision across the fault, probably driven by a regional drop in the Huang He catchment base level to the north, is more pronounced here (e.g. Li *et al.* 1997; Wang *et al.* 1995), exposing deformed rocks as fault gouge at places along the fault zone. In addition, deeply entrenched streams in the mountains on either side of that segment show particularly large cumulative offsets. The largest offset is the 85 km bend of the Huang He itself (e.g. Gaudemer *et al.* 1989), west of the Zoige marshlands, at the eastern end of the segment (Fig. 2).

North of the Rouergai–Zoige Basin, several left-stepping strands within a broad dilational jog separate the Maqen segment from the easternmost, Min Shan, segment of the Fault. This last segment stretches another 260 km, from 102.1°E to about 105°E, north of the Min Shan (Fig. 2; e.g. Chen *et al.* 1994). The active trace of the left-lateral Kunlun Fault cannot be traced any further. This makes it difficult to envision a direct link, as suggested by Zhang *et al.* (1995), between the Kunlun Fault and the Qinling–Weihe faults (e.g. Peltzer *et al.* 1985). The northeast-trending oblique-normal faults that cut the western Qinling probably absorb some strain through bookshelf faulting. However, much of the east-directed motion of central Tibet south of the Kunlun Fault is probably transformed into active thrusting and  $\sim$ EW shortening in the Min Shan and Lungmen Shan (e.g. Chen *et al.* 1994; Tapponnier & Molnar 1977; Kirby *et al.* 2000).

### 3 DEVELOPMENT OF GEOMORPHIC OFFSETS AND COSMOGENIC DATING OF DEPOSITIONAL SURFACES

#### 3.1 Landscape, climate and tectonics

The use of geomorphic offsets to determine slip-rates on active faults requires that datable morphological features first be created and then passively preserved over the observable

displacement interval (e.g. Sieh & Jahns 1984; Weldon & Sieh 1985). For the features described in this paper, the primary agents of landscape formation are glacial and fluvial processes. Such processes are modulated by climate variability. Because of the contrasting climatic environments, which affect in different ways the development of geomorphic features in the regions crossed by the Kunlun Fault, quantitative comparison of surfaces characteristics to infer ages is bound to be extremely hazardous. Direct surface dating is required.

The manner in which climate variability and tectonics interact to produce datable offsets is summarized in Fig. 4. The displacements recorded by terrace risers are necessarily minimum displacements, as they may be re-worked by subsequent fluvial erosion. For instance, flooding of the current stream which occupies T0 in Fig. 4 could cause it to temporarily reoccupy T1 resulting in lateral cutting of the T2/T1 riser, reducing the observed offset, and potentially depositing younger material on the T1 surface. Apparent diachronism may thus

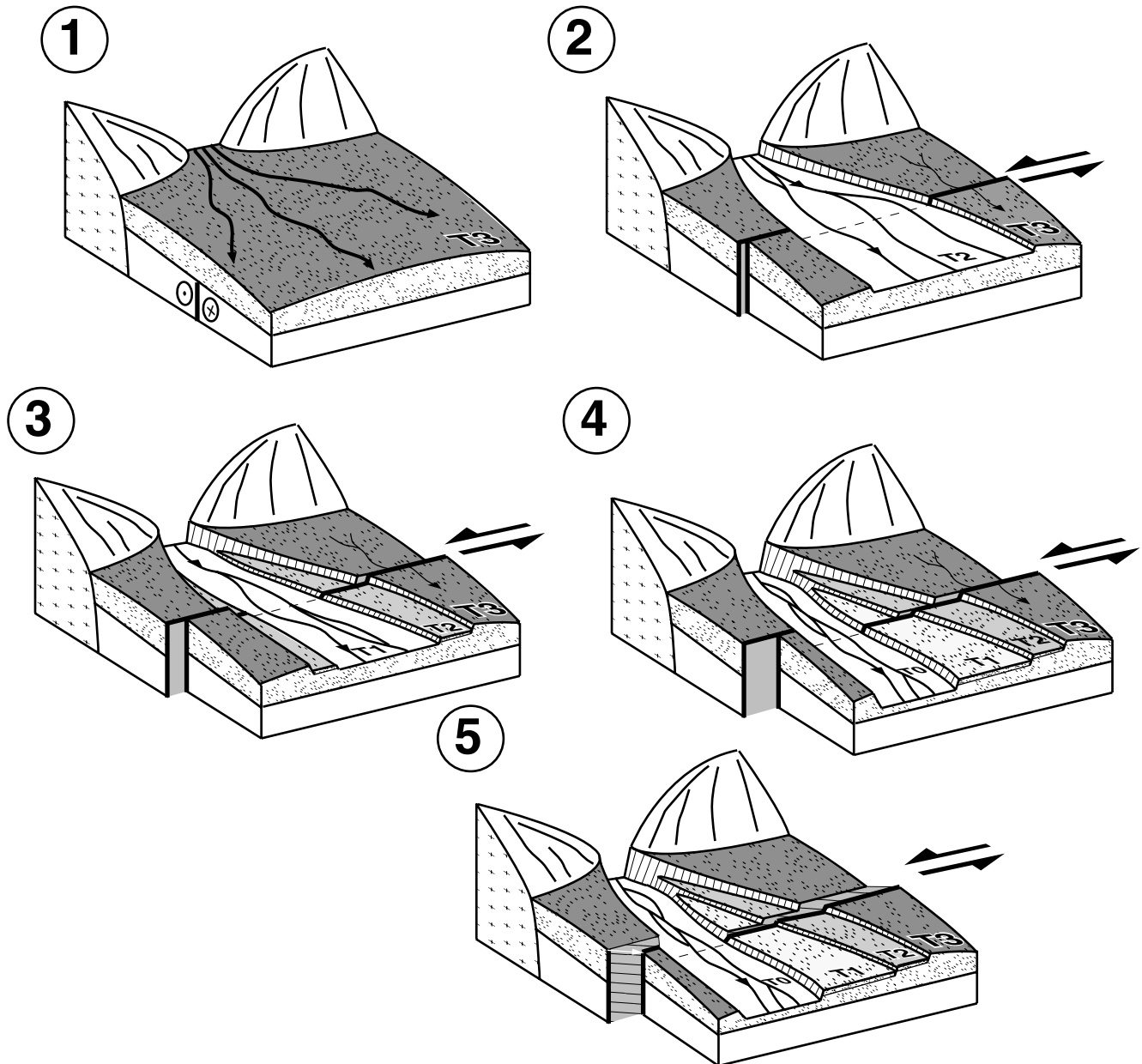


**Figure 4.** Block diagrams showing a plausible sequence of terrace emplacement and stream entrenchment disrupted by strike-slip faulting across a bajada in a range-front piedmont basin. (1) Emplacement of large fan T3 (fill) at the time of large sedimentary discharge, for instance with the advent of the Würm pluvial at the end of the glacial stage. The fault trace is buried. (2) After a period of energetic discharge, a stream incises channel T2. The T3 surface is abandoned and begins to record faulting, but the riser is constantly refreshed by lateral cutting. (3) During a new episode of entrenchment, T2 (strath) is abandoned and riser T3/T2, now a passive marker, begins to record lateral displacement. The age of T2 abandonment dates the riser offset. (4) Successive episodes of terrace bevelling and entrenchment of the stream due to climatic variation and stream profile evolution lead to the formation of several terraces whose risers are offset differently. All episodes may not be recorded by all rivers, and older terraces can be eroded by further incision (see right bank of the stream, for example). (5) A similar situation with a small vertical slip component. Vertical offset accumulates when the terrace is abandoned by the stream. Hence the vertical offset of T1 (or T2) is correlated to the horizontal T2/T1 (or T3/T2) riser offset, and correlated offsets have ages of T1, or T2, respectively.

result from short-term fluctuations in climate or sediment load that cause partial reoccupation of the lower terraces. Similarly, if the ages of various terraces represent climate events, they may yield an incomplete record as terraces can potentially be consumed by younger erosion (Fig. 4).

Opportunities for obtaining accurate slip-rates are optimal where subsequent fluvial activity has resulted in the formation of a series of inset terraces and risers within the oldest, highest fan surface level. Renewed incision indicates that the threshold between aggradation and degradation of the river bed has been crossed, a condition that may be driven by variations in sediment load and/or precipitation rate, which are in turn likely to be climate-related. While the time at which the aggradation/degradation threshold is reached at a given point along a river's course may vary—aggradation may be occurring downstream, while degradation is occurring upstream (Bull 1991)—terrace abandonment at a particular point should represent a fairly discrete temporal event. Although the number of alluvial surfaces that have been dated using cosmogenic isotopes is small (e.g. Bierman *et al.* 1995; Brown *et al.* 1998; Phillips *et al.* 1997; Ritz *et al.* 1995; Siame *et al.* 1997; Van der Woerd *et al.* 1998, 2000), previous results suggest that surface abandonment can be dated with reasonable precision, typically with relative standard deviations of about 25 per cent for 5–7 dates on fans up to 25 ka (Bierman *et al.* 1995).

### 3.2 Surface exposure (cosmogenic) dating

The accumulation of cosmogenic nuclides in near-surface samples is given by the expression

$$N(z, t) = N(z, 0) e^{-\lambda t} + \frac{P}{\lambda + \mu \varepsilon} e^{-\mu z} (1 - e^{-(\lambda + \mu \varepsilon)t}), \quad (1)$$

where  $N(z, t)$  is the concentration at depth  $z$  (cm) at time  $t$  (yr),  $P$  the surface production rate (atom g yr<sup>-1</sup>),  $\lambda$  the decay constant of the nuclide (yr<sup>-1</sup>),  $\varepsilon$  the erosion rate (cm yr<sup>-1</sup>),  $\mu$  the cosmic-ray absorption coefficient (cm<sup>-1</sup>), which is equal to  $r/L$ , where  $r$  is the density of the target rock (g cm<sup>-3</sup>), and  $L$  the absorption mean free path for interacting nuclear particles in the target rock, which is of the order of 155 g cm<sup>-2</sup>. The term  $N(z, 0)$  is the concentration of the radionuclide at the start of the irradiation interval; that is, the inherited component. The production rate,  $P$ , varies with both elevation and latitude. All of the age data presented in this work were determined from <sup>10</sup>Be and <sup>26</sup>Al, separated from quartz using the methods of Kohl & Nishiizumi (1992). The production rates are those of Nishiizumi *et al.* (1989), corrected for elevation and latitude using the scaling factors from Lal (1991). As all of our samples were collected from terrace and fan surfaces,  $z=0$ . Where erosion and inheritance are negligible [ $\varepsilon=0$ ,  $N(z, 0)=0$ ] model ages for <sup>10</sup>Be and <sup>26</sup>Al can be calculated from the expression

$$N(t) = \frac{P}{\lambda} (1 - e^{-\lambda t}). \quad (2)$$

Pre-depositional exposure or inheritance is a result of cosmic-ray exposure either during transport and storage in the fluvial system, or during exhumation of the parent bedrock surface. The more rapidly a sample is exhumed and transported, the smaller the inherited component. A rigorous and explicit treatment of the effects of inheritance in dating depositional surfaces requires subsurface sampling and reconstruction of the depth

dependence of cosmogenic nuclide concentration, accounting for the effects of variable inheritance and grain size (Anderson *et al.* 1996; Hancock *et al.* 1999; Repka *et al.* 1997). For instance, if inheritance is constant from sample-to-sample (a special case which is probably only obtained when inheritance is negligible), then extrapolation of a cosmogenic nuclide-concentration depth profile to a depth at which the sample is effectively shielded from cosmic-ray exposure (at  $z > 3$  m, the effective spallogenic production rate approaches zero) will yield the inherited component. While subsurface sampling has not been performed in the current study, we show, based upon the population statistics of our surface ages and the high fluvial gradient and short transport distance, that pre-exposure in our samples was in general small.

## 4 RATES OF SLIP AND SEISMIC BEHAVIOUR OF THREE SEGMENTS OF THE KUNLUN FAULT

In the following sections, we present the detailed, quantitative geomorphic study of six sites, spread along three segments of the Kunlun Fault.

### 4.1 Western, Xidatan–Dongdatan segment

#### 4.1.1 Geologic and geomorphic framework

This segment strikes N80°E to N90°E, crosscutting the long and narrow Xidatan–Dongdatan pull-apart trough (Fig. 5). The trough is floored by broad Quaternary bajadas fed by separate drainage catchments on either side of a gentle saddle (Fig. 5a). Both drainages flow north, from headwaters in the Burhan Budai mountain range, just south of the bajadas. This ice-capped range peaks above 6000 m (Fig. 5a), and is chiefly built of strongly folded turbidites and phyllites belonging to the Triassic Songpan Garze terrane of eastern Tibet (Chang *et al.* 1986). The Kunlun Fault separates this terrane from Lower–Middle Palaeozoic metamorphic rocks intruded by Mesozoic granites to the north (Coward *et al.* 1988; Mock *et al.* 1999). East and west of Xidatan, the gneiss lens along the fault has yielded lower Cretaceous ages (Arnaud *et al.* 1997). Present-day glaciers flowing down the gentler, broader north slope of the Burhan Budai range stop short of the Xidatan trough at elevations between ~5500 and ~4800 m. There is no clear evidence of recent glacial deposits in Xidatan; evidently the ice tongues in the latest Pleistocene did not extend much farther than they do today (Kidd & Molnar 1988). In particular, there is no geomorphic indication that they crossed the active Kunlun Fault trace at that time (e.g. Lehmkuhl *et al.* 1998).

From west to east, the fault angles away from the southern range front, cutting across fans whose coalescence has built the north-sloping bajadas. The fault is marked by large, stepping sag-ponds and pressure ridges in the fanglomerates (Kidd & Molnar 1988). Commonly, risers of inset alluvial terraces in the fans are horizontally offset 10–100 m by the fault (Kidd & Molnar 1988; Fig. 5). At places, there is a slight vertical component of slip, usually related to small changes in strike (e.g. Gaudemer *et al.* 1995b; Peltzer *et al.* 1988b). For instance, in the eastern part of Xidatan metres of uplift north of the fault have led to stream damming and ponding (Fig. 5c). Despite the seismically disrupted morphology, however, there is no historical or instrumental record of recent earthquakes in the

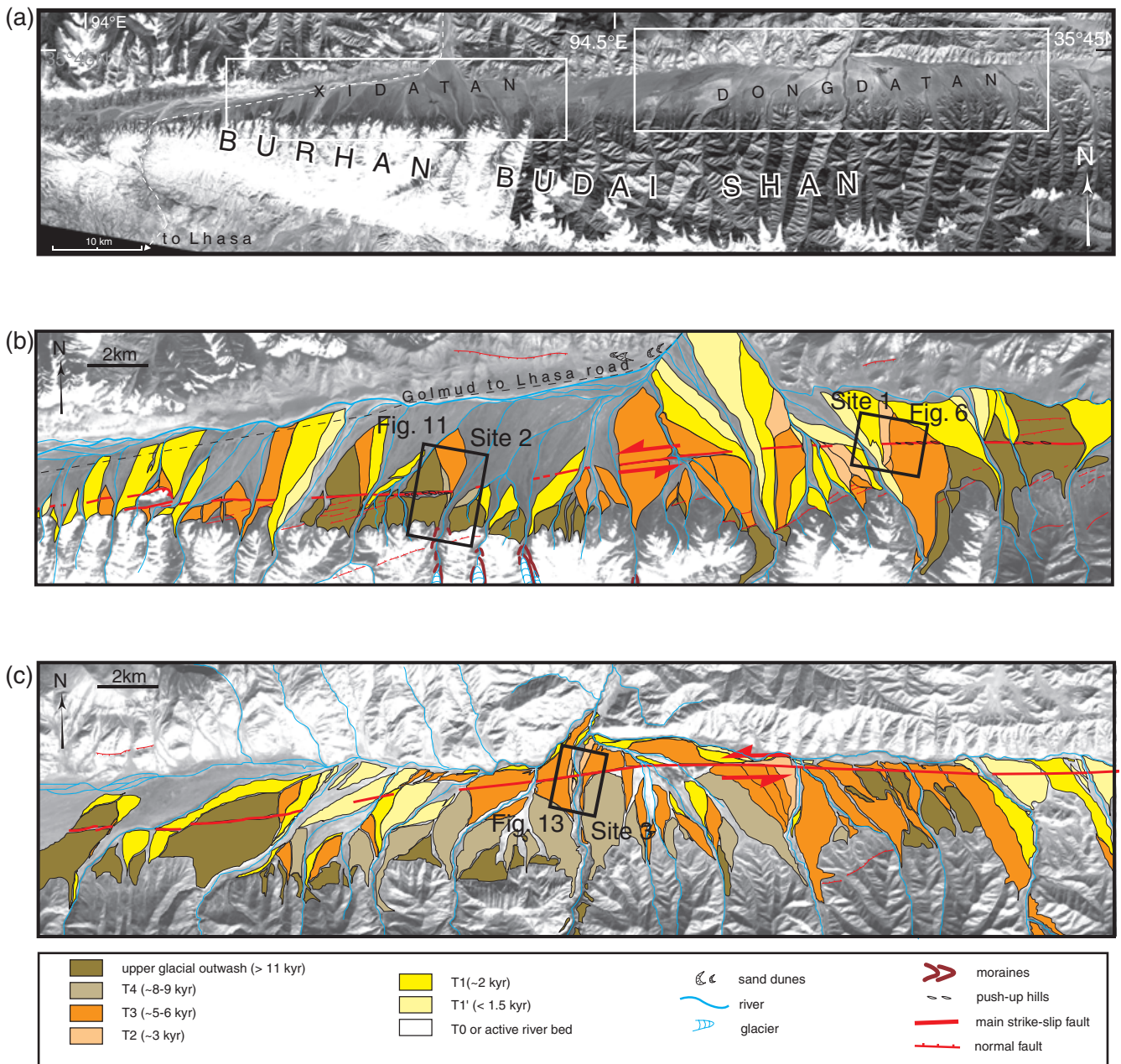


**Figure 5.** (a) SPOT image (KJ237-278 and KJ239-278) mosaic showing the Xidatan segment of the Kunlun Fault. White dashed line indicates the road from Golmud to Lhasa, which crosses the Burhan Budai range just north of Kunlun Pass. The main branch of Kunlun Fault strikes N80–90°E, from the western end of Xidatan valley to the northeastern corner of Dongdatan valley. A clear trace of Kunlun Pass Fault is also visible south of the Burhan Budai ice-capped crest line. White rectangles are the locations of Figs 5(b) and (c). (b) Geomorphic map of alluvial fans and terraces cut by Kunlun Fault in central Xidatan. Bold boxes indicate the locations of sites 1 and 2. The fault trace is fairly continuous across bajada, except in the most recent alluvial surfaces where it vanishes. Discontinuous normal fault-scarps are visible north and south of the valley at the foot of ranges. Seven alluvial terrace levels can be distinguished and correlated on the basis of relative elevation, incision, and hence age, by combining field evidence with SPOT image analysis. (c) Geomorphic map of alluvial fans and terraces cut by Kunlun Fault in central Dongdatan. The bold box indicates the location of site 3.

area. Moreover, the trace of the fault vanishes in most low-level terraces, up to 2 m above the seasonal to centennial flood plains, implying the rare occurrence of great earthquakes.

Locally, the mean elevation of the permafrost line is about 4300 m (Derbyshire 1987). The apices of the stream fans stand roughly at that same elevation, while the bottom of the valley remains above 4000 m a.s.l. in Xidatan, and above 3700 m in Dongdatan. In general, streams are entrenched inside inset

terraces along the side or in the middle of their largest, oldest fans, whose surfaces are sprinkled with loess (light grey on the SPOT image, Fig. 5a). Such setting is typical of most large, north-flowing streams in Xidatan and Dongdatan, which appear to have had similar, recent histories of aggradation and incision. Large alluvial fans first formed at the outlet of the lowermost moraines. These old fan surfaces were then incised by, and hence protected from further action of, the stream, and consequently

recorded the largest cumulative deformation due to motion on the fault, such as the large—up to 15 m deep and 40 m high—sag-ponds and pressure ridges noted by earlier workers (Kidd & Molnar 1988; Figs 6(a) and 7(a)). The stepwise, northward progradation of deposition is due to stream profile adjustment, in tune with postglacial climate change. The wet, warm period that followed deglaciation—the Early Holocene optimum, now recognized in various parts of Asia (e.g. Gasse *et al.* 1991; Lavé 1997; Liu *et al.* 1998; Pachur *et al.* 1995)—probably led to high-energy transport in the upper reaches of the streams, and the

deposition of large amounts of debris at the foot of the Burhan Budai range. During the following, drier period, the streams re-established their former profile through incision (Bull 1991), leading to the demise of the stepping strath terraces.

First-order mapping of the different terrace levels deposited by streams along the Burhan Budai Shan (Figs 5b and c) was done by combining several types of evidence. The terraces and risers were identified using panchromatic SPOT images (pixel size = 10 m) and air photos. The relative ages of the terraces were derived from their relative heights, from the

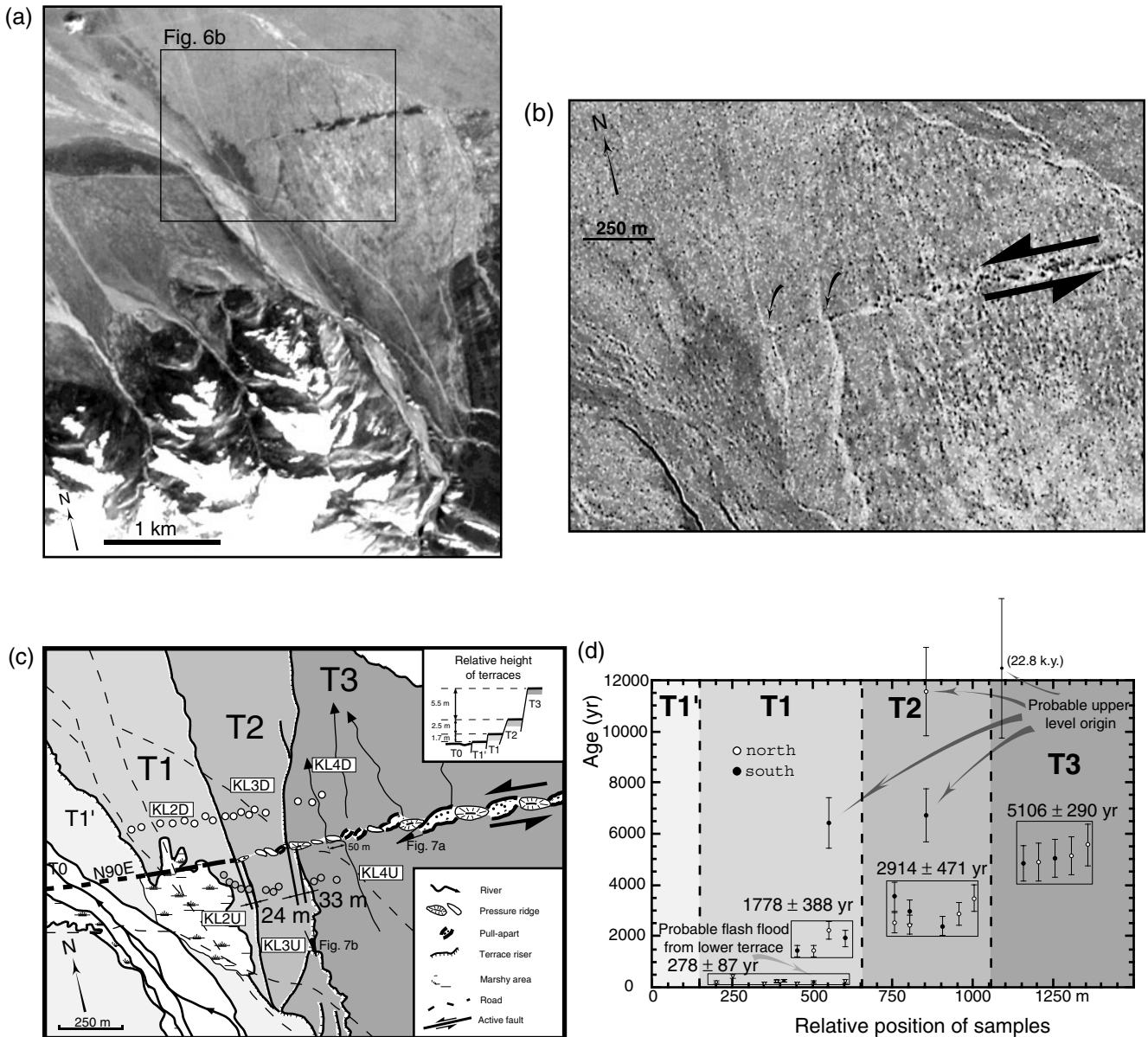


**Figure 6.** (a) Enlargement of the panchromatic SPOT image KJ237-278 of site 1. The older fan surface (T3) is clear from its spotted, light-grey to white hue. Stepping earthquake pressure ridges and sag-ponds (enhanced by shadows) are larger on T3 than on T2, and disappear altogether on T1 and T1'. The box corresponds to part (b). (b) Enlargement of CORONA satellite image DS1048-1054DA094 scanned at 2400 dpi with a pixel size of 3.8 m. Black arrows show the offsets of the two principal terrace risers. (c) Schematic interpretation of images. Alluvial surfaces are numbered as a function of increasing height and age (inset), starting in the active stream flood-plain (T0) to the left. Riser offsets were measured in the field, on air photos and the SPOT image. Fist-size quartz pebbles were sampled on top of the main alluvial surfaces, south (grey circles) and north (white circles) of the fault trace. (d) Plot of sample ages, for each terrace, in relative position, from west to east. For each terrace level, samples were grouped and a mean age calculated (boxes and bold numbers). Light and dark arrows indicate a flash-flood and outliers, respectively. Note the slight, systematic decrease in ages (~1000 yr) on each terrace from east to west.

amount of tectonic strain recorded, and from the appearance of their surfaces (weathering, soil development, erosion, eolian deposition; e.g. Bull 1991).

#### 4.1.2 Site descriptions: riser offsets, inset terrace ages, slip-rates

*Site 1:* There are three main terrace levels at site 1 (Fig. 6), numbered as a function of increasing height and age (Fig. 6c). T0 is the active stream flood plain, T1 the terrace last abandoned by the stream, T1 a first strath terrace  $\sim 1.70$  m above the stream bed, and T2 a second strath terrace,  $\sim 2.5$  m above T1. T3 is the highest level, corresponding to the ancient fan surface, about 5.5 m above T2. The surface of T3 may be in part diachronous and is incised by smaller gullies or rills, but it bears no large riser in the area we sampled. Although T1 is now clearly abandoned by the stream, its western riser is not well defined, and its surface is occupied by a wet, marshy area south of the fault trace (dark region on the SPOT image, Fig. 6a). On all the surfaces, the recent deposits are composed of relatively small, well-rounded and sorted pebbles and cobbles, at places below a thin soil and turf cover (Fig. 7b). Both of the principal risers (T2/T1 and T3/T2) are offset by the fault (Figs 6 and 7b). Our measurements of the offsets (with a tape in the field, corroborated by air photo, Corona and SPOT image interpretations) are  $24 \pm 3$  m and  $33 \pm 4$  m, respectively. The oldest, highest

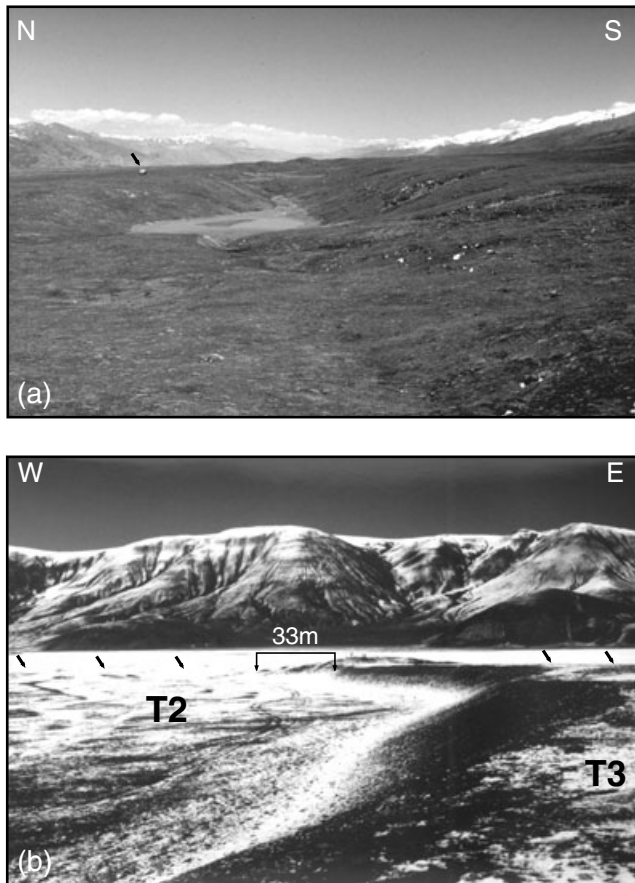


**Figure 7.** (a) View, looking east from site 1, of the large sag-pond due to cumulative deformation by several large earthquakes (Toyota black arrow, gives scale). (b) View, looking north from the top of T3, upstream from site 1, of the dogleg, sinistral offset of the T3/T2 riser.

riser T3/T2 is offset more (by about 30 per cent) than the more recent T2/T1 riser, closer to the river. A small seismic pull-apart sag just upslope from the fault trace on T2 and a large pressure ridge on T3 (Fig. 6c), sliced by three steep, en échelon scarples within the dogleg offset of the T3/T2 riser (Fig. 7b), make more accurate measurements of the offsets difficult. The particularly large sags and pressure ridges on T3 (Fig. 6a) imply cumulative ground deformation by several earthquakes. One gully channel on T3 is offset by as much as  $\sim 50$  m (Fig. 6c). On T2 such features are smaller and smoother. There are no clear mole tracks on T1 (Fig. 6b).

We collected fist to subfist size, or fragments of, quartz pebbles weighing 300 g at most on the surfaces of terraces T1, T2 and T3 along two parallel traverses, about 100 m up- and down-slope from the fault (Fig. 6c). 29 samples were processed: 13 on T1, 10 on T2, and six on T3.

The concentrations of  $^{26}\text{Al}$  and  $^{10}\text{Be}$  are listed for each sample in Table A1 in Appendix A (see also the  $^{26}\text{Al}/^{10}\text{Be}$  age ratios in Fig. 8). With the exception of samples less than 500 years old, the  $^{26}\text{Al}$  and  $^{10}\text{Be}$  ages are concordant to within 10 per cent, consistent with simple exposure histories. The samples showing the greatest disparities between the  $^{26}\text{Al}$  and  $^{10}\text{Be}$  model ages belong to the youngest population on the lower terrace (T1), mostly north of the fault trace. The low cosmogenic nuclide abundance in these samples (*ca.*  $2 \times 10^4$  atom  $\text{g}^{-1}$ ) results in a large relative error on the age. Bierman *et al.* (1995) observed similarly large uncertainties on the ages of samples with similar nuclide concentrations. Except as noted in the Table, we will use a weighted mean of the  $^{26}\text{Al}$  and  $^{10}\text{Be}$  ages in the discussion below.

The ages obtained for each terrace level identified and sampled in the field are in general similar, regardless of whether the sample lies upstream or downstream of the fault. Hence, for each terrace level, we group the sample populations from both sides of the fault. Fig. 6(d) shows the mean Al–Be ages of samples on each terrace, plotted in their relative position along the fault, from west to east.

The youngest samples, with mean ages ranging from  $\sim 200$  to  $\sim 500$  yr are found on the surface of T1, presently about 2 m above the riverbed, all the way to the T1/T2 riser. We interpret these samples to reflect the occurrence of a single, recent depositional event, probably a centennial flash flood that invaded and washed T1, re-depositing material from the flood

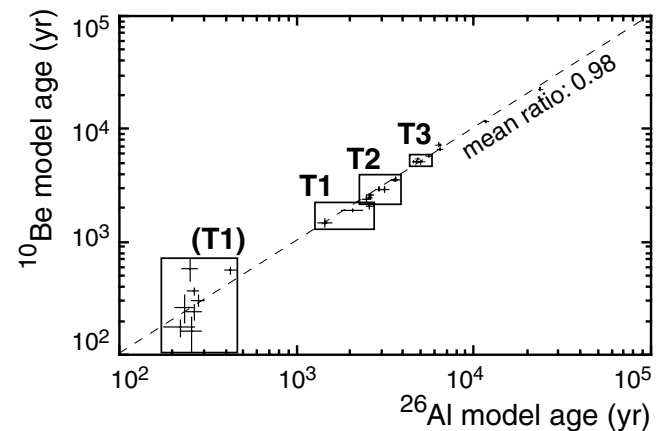


**Figure 8.**  $^{10}\text{Be}$  versus  $^{26}\text{Al}$  model ages for samples collected at site 1. The large scatter in the youngest ages (200–400 yr) is due to small nuclide concentrations.

plain onto its surface. This would support the inference that strong water flow across T1 must have eroded earthquake mole tracks, which are unclear on this surface. Four other samples on the eastern half of that terrace yield ages we believe to be closer to the time at which its surface ceased to be the permanent flood plain of the river ( $1778 \pm 388$  yr; Fig. 6d). Evidently, the flash flood that transported the  $\leq 500$  yr old samples did not rework the entire surface of T1 and did not modify the offset of the T1/T2 riser by the fault.

While most sample ages on each terrace show no overlap with those on others (Fig. 6d), and tend to cluster around distinct, mean values ( $1778 \pm 388$ ,  $2914 \pm 471$  and  $5106 \pm 290$  yr), which increase with elevation above the stream bed, four samples are much older than all the others. One, on T1, is  $> 4$  kyr older than the  $1778$  yr mean age; two, on T2, are  $> 4$  and  $> 8.5$  kyr older than the  $2914$  yr mean age; and the oldest, on T3, is  $> 17$  kyr older than the  $5106$  yr mean age. These four outliers clearly have experienced much longer exposure histories than the other samples, and most probably represent reworked material from older deposits upstream. The oldest cobble (22.8 ka) may have originated in a moraine of the Last Glacial Maximum (LGM,  $\sim 20$  ka).

One particularly serious problem in the cosmogenic dating of alluvial surfaces, recognized by previous authors (e.g. Anderson *et al.* 1996; Brown *et al.* 1998; Molnar *et al.* 1994; Repka *et al.* 1997; Ritz *et al.* 1995) is the possibility of nuclide accumulation prior to deposition. One way to assess the presence of such inherited nuclides is to date pebbles from the active riverbed. As the active riverbed has yet to be abandoned, it has zero effective age, and cosmogenic nuclide concentrations in its pebbles are therefore entirely derived from pre-depositional exposure. The validity of such an approach depends upon whether the sediment source and depositional style in the active riverbed are representative of those of the older, abandoned terraces.

This seems to be the case for the inset terraces discussed here. While we have not sampled the active stream bed, T0, the groups of  $\sim 200$  to  $\sim 500$  yr old samples found on terrace T1 appear to have been derived from either T0 or T1', and place an upper limit on the inherited cosmogenic nuclide concentration. The relatively small inherited component indicates that pebble or cobble exposure either in the bedrock surface or during transport should have been minimal, in general, which is consistent with the relatively steep and small catchment upstream from the site and short distance between the range crest and the sampled terrace surfaces ( $\leq 10$  km, with an average slope gradient of  $\sim 4^\circ$ ).

The mean ages (exclusive of the outliers discussed above, and with no correction for inheritance) of T1, T2 and T3 are  $1778 \pm 388$ ,  $2914 \pm 471$  and  $5106 \pm 290$  yr, respectively (Fig. 6d). At a more detailed level, within each sample set on each terrace, there appears to be a decrease of  $\sim 1000$  yr in age from east to west. This might reflect progressive terrace abandonment westwards by the stream, but more data are needed to confirm this inference. The dispersion of ages within the sample set for each terrace may be taken to indicate that their surfaces still evolved while the stream abandoned them, with diachronic mixing by waterflow in the upper several tens of centimetres near the surface. Bioturbation, cryoturbation and variable inheritance might also contribute to such dispersion. If one took the youngest samples closest to the riser tops on T1, T2 and T3 as more representative of terrace ages before

complete abandonment, then such ages would be  $1452 \pm 237$ ,  $2414 \pm 375$  and  $4852 \pm 702$  yr, respectively (Table A1).

Strath terrace risers are constantly rejuvenated by river flow along their base. Consequently, only when the terrace level at the base of a riser is abandoned can this riser begin to act as a passive marker and record displacement by a fault. We thus relate the offsets of the T3/T2 and T2/T1 risers to the ages of T2 and T1, respectively (e.g. Bull 1991; Gaudemer *et al.* 1995b; Weldon 1986). The Kunlun Fault would therefore have offset the T3/T2 riser by  $33 \pm 4$  m in  $2914 \pm 471$  yr, and the T2/T1 riser by  $24 \pm 3$  m in  $1778 \pm 388$  yr (Fig. 9). Both offsets yield fairly consistent slip-rate values ( $11.3 \pm 3.2$  and  $13.5 \pm 4.6$  mm yr $^{-1}$ ) which constrain the Late Holocene left-slip-rate along the fault in east Xidatan to be  $12.1 \pm 2.6$  mm yr $^{-1}$  (Fig. 9). In addition, the 50 m offset of the small gully on the surface of T3, whose incision must post-date somewhat the  $5106 \pm 290$  yr age of this terrace, but is likely to be much older than the time at which T2 was abandoned, yields a minimum slip-rate of  $9.2$  mm yr $^{-1}$ , consistent with the above values (Fig. 9).

*Site 2:* Site 2 is located  $\sim 10$  km west of site 1 (Fig. 5b), where the fault trace crosses a large fan and inset terraces on the left bank of a stream, at the outlet of a glacial valley,  $\sim 2$  km down from the present terminus of the glacier (Figs 10 and 11). Remnants of morainic ridges bound the valley sides upstream from the range front. The western lateral moraine shoulders the western half of the entrenched fan apex (Fig. 11).

There are four main terrace levels at this site (Fig. 11c). T0 is the active stream flood plain, T3 a first strath terrace,  $\sim 5$  m above the stream bed, and T4, a second strath terrace,  $\sim 4$  m above T3. The highest terrace level, T5, corresponds to the ancient fan surface, about 2 m above T4. The surface deposits are similar to those at site 1. The two principal fossil risers, T4/T3 and T5/T4, are offset by the fault (Figs 11b and c). Our measurements of the two offsets (with a tape in the field, corroborated by air photo, Corona and SPOT image interpretations), are  $70 \pm 5$  m and  $110 \pm 10$  m, respectively (Fig. 11c). Back-slipping the terrace morphology on either side of the fault by those amounts restores the continuity and shapes of the two risers (Fig. 12). As at site 1, the oldest, highest riser (T5/T4) is offset more than the more recent riser (T4/T3). Assuming a constant slip-rate along the fault, the observed horizontal

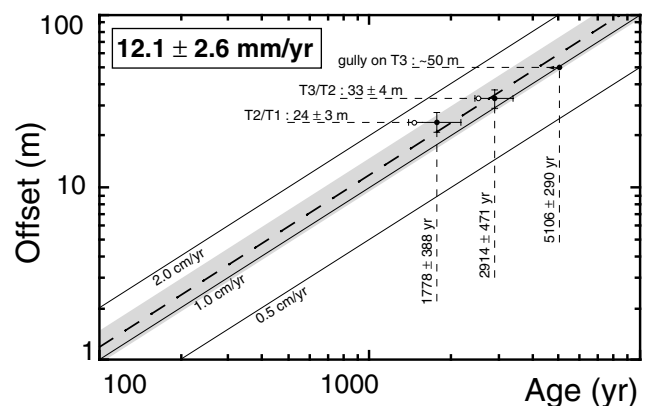


**Figure 9.** Late Holocene left-slip-rate at site 1, as deduced from the offsets of the T3/T2 and T2/T1 risers. Open circles correspond to the ages of the two youngest samples on each terrace, and bold circles to the average age.

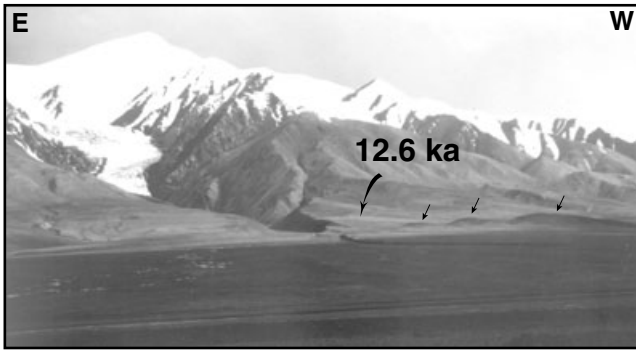


**Figure 10.** View, looking south, of site 2. The fault trace is marked by large pressure ridges on the left bank of the stream fed by melting glacier in the background. Snow- and ice-covered summits are  $\sim 6000$  m high, and the bajada in the foreground is  $\sim 4000$  m a.s.l. The stream first formed a large fan after the onset of postglacial warming (cosmogenic age  $\sim 12\,600$  yr BP), and then deposited two inset terraces during entrenchment ( $\sim 8100$  and  $6200$  yr BP; see text and Fig. 11).

offsets imply that the lowest terrace at site 2 (T3) should be older than, or at most coeval with, the highest terrace dated at site 1 (T3, orange colour). Neither of the lower terraces at site 1 (T2, T1) thus appear to have been preserved at site 2. The relative height of the terraces and the very large pressure ridges due to cumulative displacement across T5 concur to suggest that the terraces here are older than those at site 1.

Samples were collected on the surfaces of T3, T4 and T5 along two traverses roughly parallel to the fault, up- and down-slope from it (Fig. 11c). 23 samples were processed: 12 on T3, six on T4 and five on T5. The concentrations of  $^{26}\text{Al}$  and  $^{10}\text{Be}$  are listed for each sample in Table A2.

Like the samples from site 1, most samples have concordant  $^{26}\text{Al}$  and  $^{10}\text{Be}$  ages, consistent with simple exposure histories. Four samples (KL15D-2, KL15D-7, KL15U-5 and KL16U-6) have discordant ages (Al/Be age ratio  $< 0.7$ ) (Fig. A1, Table A2). Given the relative youth of the samples, it is unlikely that such discrepancies result from complex burial histories, or from erosion. Rather, they probably reflect analytical problems. Comparison of the  $^{10}\text{Be}$  and  $^{26}\text{Al}$  data from samples that yield discordant ages with those of concordant samples suggests that it is the  $^{26}\text{Al}$  data from the discordant pairs that are problematical. Thus, for those four discordant samples we consider only the  $^{10}\text{Be}$  age in the discussion below.

As at site 1, the ages obtained for each terrace are similar regardless of whether the sample is upstream or downstream from the fault. Hence, for each terrace level we group the sample populations from both sides of the fault (Fig. 11d). One sample on T3 (KL15U-5) and two on T4 (KL16U-2 and KL16U-3) are older than the mean ages of T3 and T4 and could have been washed down from T5. Only one sample (KL17U-7) has an age very different (24.7 ka) from those of all others, comparable to that of KL4U-1 at site 1, and may have originated in the LGM moraine less than 2 km upstream (Fig. 11a).

The mean ages of T3, T4 and T5, excluding the outliers discussed above, as well as KL15D-3 for which only an Al age is determined, are  $6276 \pm 262$ ,  $8126 \pm 346$ , and  $12\,614 \pm 2303$  yr, respectively. As at site 1, we relate the offsets of the T5/T4 and T4/T3 risers to the ages of T4 and T3, respectively. The Kunlun Fault would therefore have offset the T5/T4 riser by  $110 \pm 10$  m in  $8126 \pm 346$  yr, and the T4/T3 riser by  $70 \pm 5$  m in

$6276 \pm 262$  yr. Both offsets yield compatible slip-rate values ( $13.5 \pm 1.8$  and  $11.2 \pm 1.3$  mm yr $^{-1}$ , respectively) which constrain the Early Holocene left-slip-rate along the fault at site 2 in west Xidatan to  $11.9 \pm 1.0$  mm yr $^{-1}$ .

**Site 3:** This site is located in the middle part of Dongdatan, on the main and most deeply entrenched stream crossing the fault (Figs 5c and 13). The stream originates 16 km to the south and has one of the largest catchments among streams flowing across the Dongdatan valley. Fan deposition and incision followed a pattern similar to the other sites, but with the latest incision phase lowering by  $\sim 30$  m the  $\sim 200$  m wide stream bed. We mapped two main, high-level, inset terraces (T2, T3) below the younger fan on the left bank of the stream. T2 is about 30 m above the active stream T0 (Fig. 13c). The highest level T3, about 4 m above T2, is divided into sublevels T3-1, T3-2 and T3-3. The fault trace at this site is clearly outlined by a south-facing, 4–4.6 m high scarp, illuminated by the sun on the SPOT image (Fig. 13b). Since the drainage and terrace surfaces slope perpendicularly to the fault, such an upstream-facing scarp must result from a small component of vertical throw ( $\sim 6$  per cent) on the fault. Owing to the deep entrenchment of the stream, the terraces south of the fault have been degraded by the regressive incision of small, tributary gullies channelled along the base of the fault scarp and of some terrace risers (Fig. 13b).

Two risers (T3-2/T3-1 and T3-3/T3-2) are offset  $47 \pm 5$  m and  $68 \pm 5$  m, respectively (Fig. 13c). Samples were collected from the surfaces of terraces T3-1, T3-2 and T3-3 along two traverses parallel to the fault, about 200 m up- and down-slope from it (Fig. 13c). 41 samples were processed: 12 on T3-1, 12 on T3-2 and 17 on T3-3.  $^{26}\text{Al}$  and  $^{10}\text{Be}$  concentrations are listed for each sample in Table A3, and  $^{26}\text{Al}/^{10}\text{Be}$  age ratios are plotted in Fig. A2. 37 samples have  $^{26}\text{Al}$  and  $^{10}\text{Be}$  ages consistent with simple exposure histories. One sample (KL7U-4) has a large  $^{26}\text{Al}/^{10}\text{Be}$  age discrepancy, and for one sample (KL6U-5) low ion currents and small sample size prevented the determination of an  $^{26}\text{Al}$  age. Excluding these two samples, we use the mean Al–Be ages in the discussion below.

For each level we group as elsewhere the sample populations from both sides of the fault (Fig. 13d). Six samples are clear outliers and must have experienced longer exposure histories. Three (KL6U-1, KL6D-2, KL6D-3), with model ages between 10 and 17 ka, are found on the lower terrace sublevel, T3-1. One (KL7D-1), on T3-2, yields the oldest age at this site ( $\sim 41$  ka), and two (KL8U-15 and KL9U-1), on T3-3, ages of  $\sim 28$  and 11 ka. Five other samples with ages of 7.5–8.3 ka (two on T3-1: KL6U-4 and KL6D-4, and three on T3-2: KL7D-3, KL7D-5 and KL7D-6) are also significantly older (95 per cent confidence level using a  $\chi^2$  test) than other samples on either terrace and may have been reworked from the older fan upstream (Fig. 13a). We do not use these 12 older samples to calculate the mean ages of the terraces (Fig. 13d). Note that, if the older samples were previously exposed at a higher elevation, the appropriate production rates should be higher than those we used to calculate their model ages. As such, the model ages presented for these outliers will probably overestimate the ages of their source deposits, and are not interpreted as the real ages of terraces or moraines above the sampling site.

In contrast with the spatial distribution of ages at the two other sites, the sample age distributions on the individual

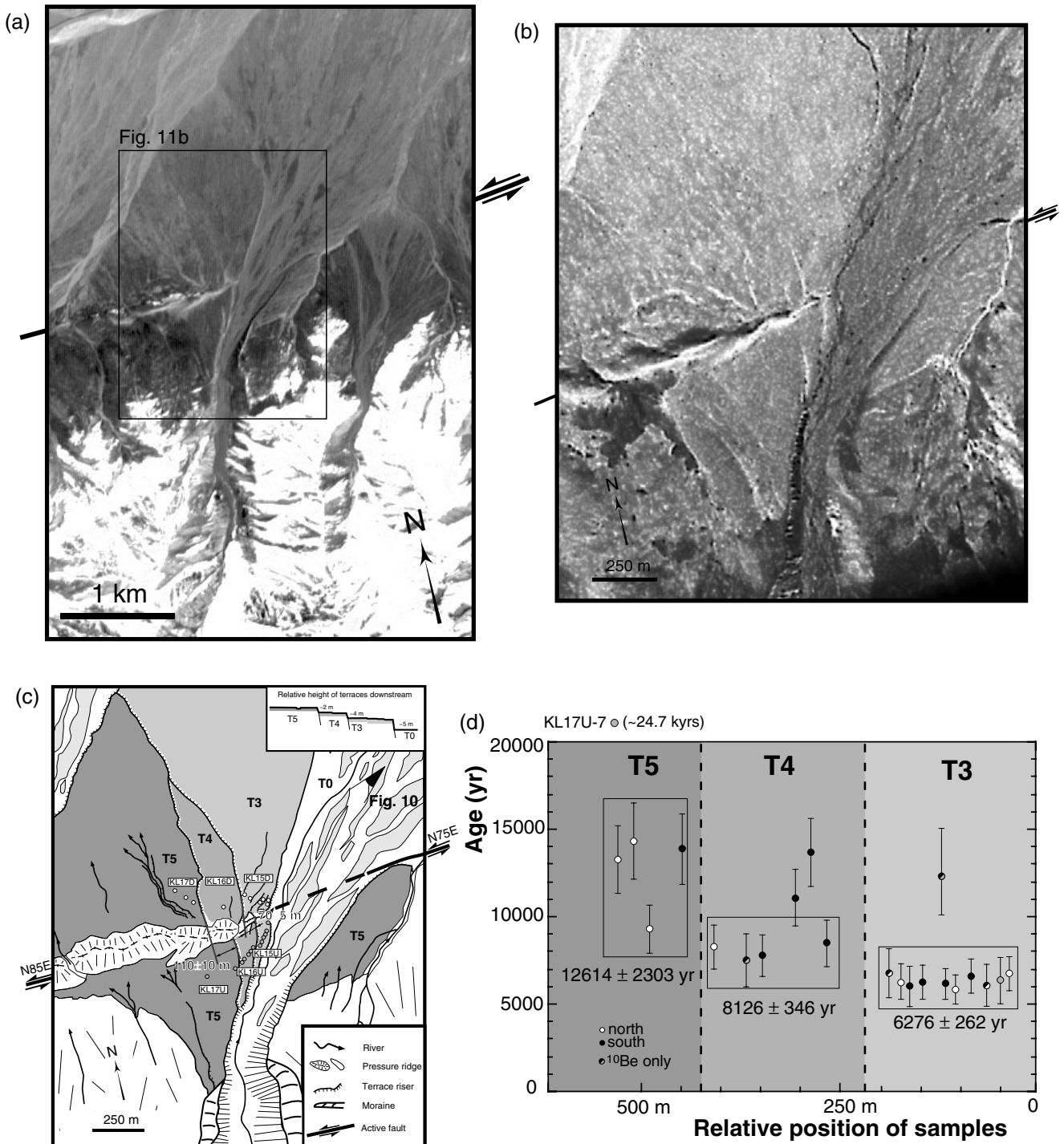


**Figure 11.** (a) Enlargement of panchromatic SPOT image KJ237-278 of site 2. The fault trace is marked by snow-covered pressure ridges on the old fan surface. This surface merges with the frontal moraine, which has been breached and deeply incised by the river. Incision has led to the formation of inset terraces that are offset several tens of metres by left-lateral movement on the fault. The black rectangle corresponds to part (b). (b) Enlargement of CORONA satellite image DS1048–1054DF094 scanned at 2400 dpi with a pixel size of 3.8 m. (c) Schematic interpretation of images. Alluvial surfaces are numbered as on Fig. 5. Riser offsets were measured in the field and on CORONA and SPOT images. The fault trace is marked by large pressure ridges. Fist-size quartz pebbles were sampled on top of the main alluvial surfaces, south and north of the fault trace (grey and white circles, respectively). (d) Plot of sample ages, for each terrace, in relative position, from east to west. For each terrace level, samples were grouped and a mean age calculated (boxes and bold numbers).

terraces here overlap, particularly for the two highest terrace levels, T3-2 and T3-3. For these two levels the mean values ( $6043 \pm 553$ ,  $5884 \pm 537$  and  $6403 \pm 967$  yr, Fig. 13d) are statistically indistinguishable, even though they are separated

by a 2–3 m high riser (Fig. 13c, inset). The most plausible explanation is that the uppermost terraces were rapidly emplaced, in episodic high-energy depositional events, in the span of only a few centuries. This depositional environment

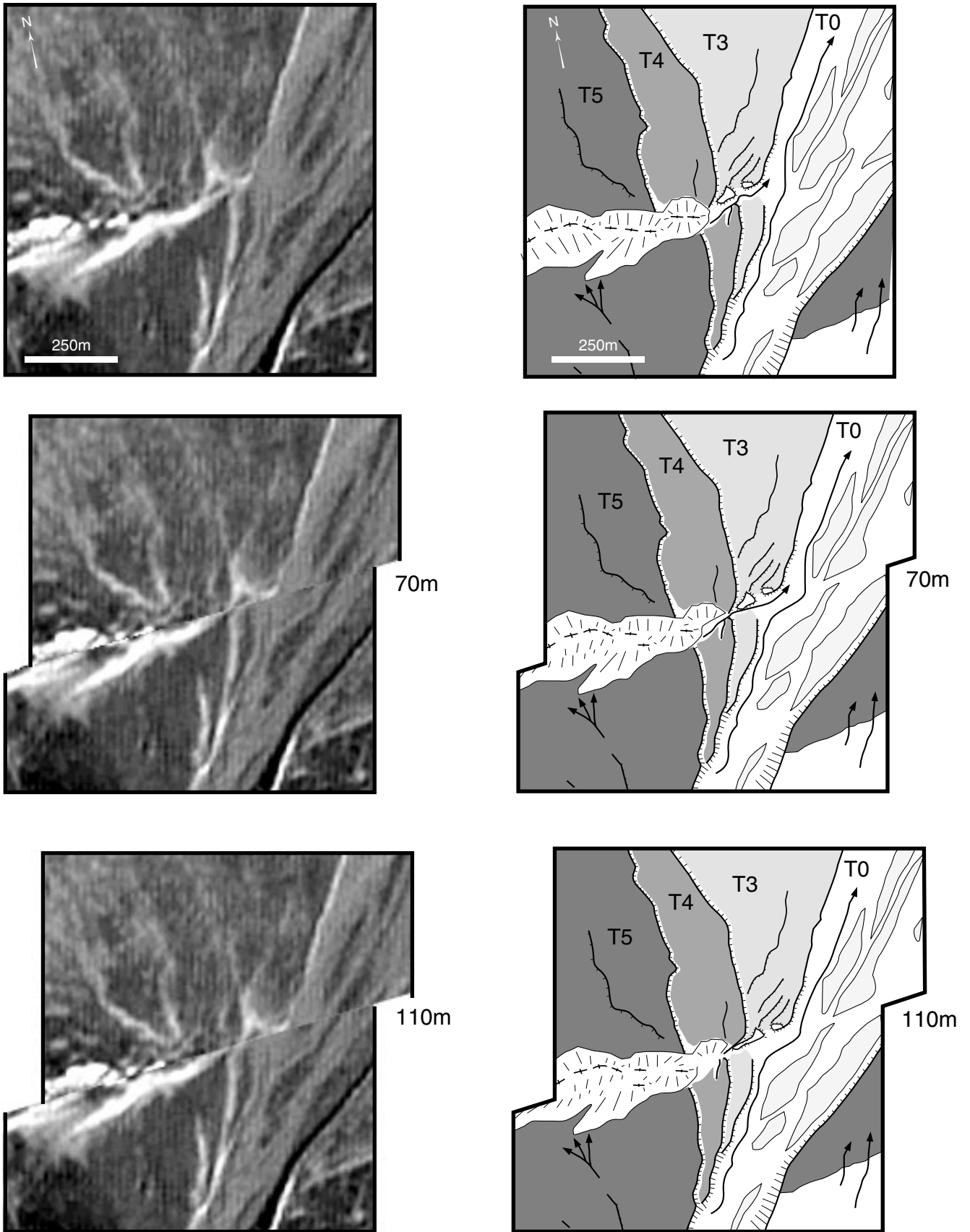
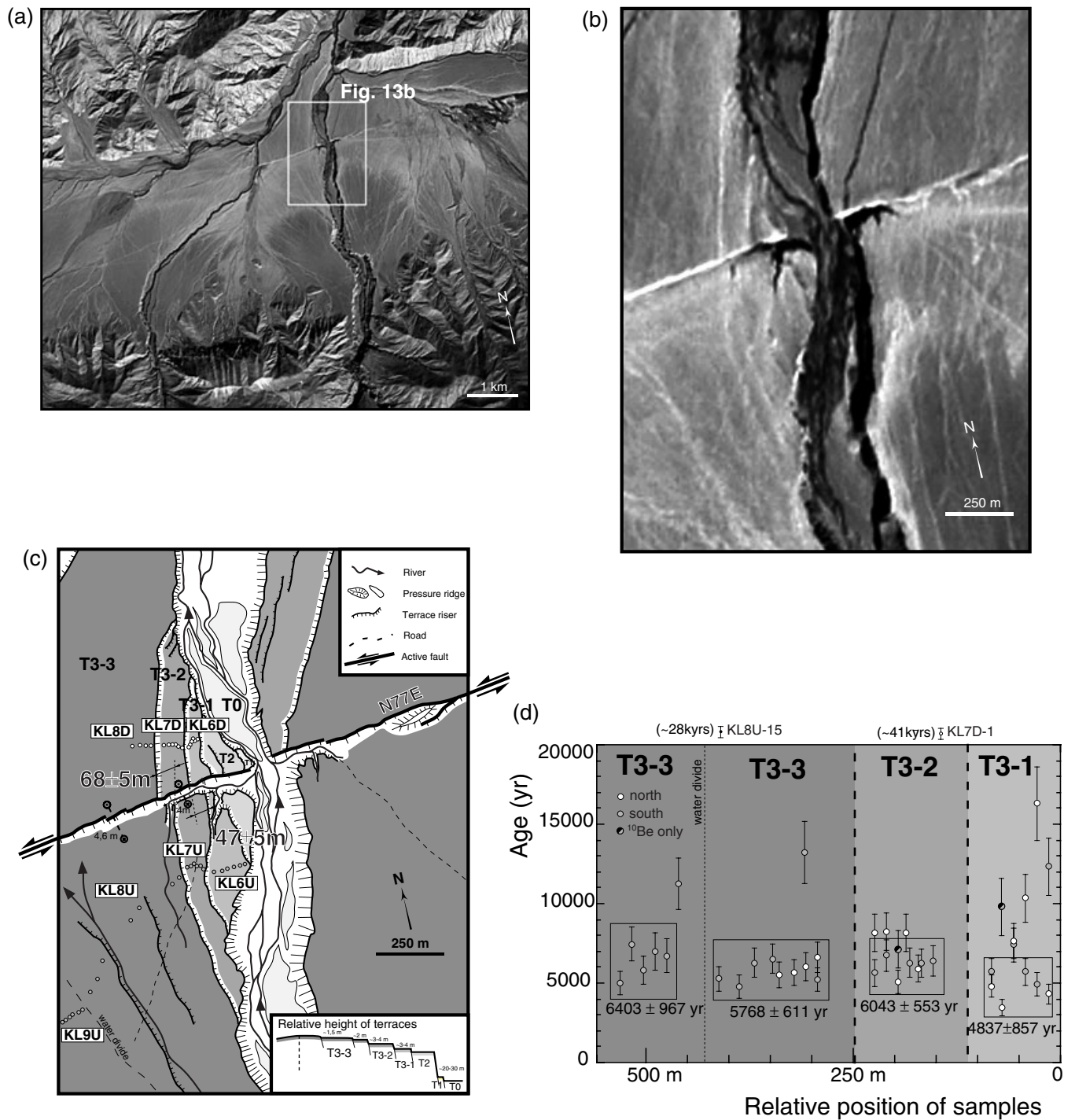


Figure 12. Best fit between blocks offset by the fault in order to adjust terrace risers T4/T3 and T5/T4. Left, SPOT image enlargement; right, schematic interpretation.



**Figure 13.** (a) Location of site 3 on panchromatic SPOT image KJ239-278. The largest, north-flowing stream in the middle of the image is entrenched a few tens of metres into a large ancient fan. Note the straight trace of the strike-slip fault and the left-lateral offset of the main stream. (b) Enlargement of the SPOT image of site 3. The fault trace is marked by south-facing sunlit scarp. The stream has deposited several inset terraces, whose risers are left-laterally offset. (c) Schematic interpretation of the image enlargement in (b). Alluvial surfaces are numbered as on Fig. 5. Riser offsets were measured in the field and on the SPOT image. Quartz pebbles were sampled on top of the main alluvial surfaces, south and north of the fault trace (white and grey circles, respectively). The inset shows the approximate relative height of the terraces. (d) Plot of sample ages in relative position for each terrace. For each terrace level, samples were grouped and a mean age calculated (boxes and bold numbers). T3-3 is separated into two subsurfaces on either side of the water divide of the fan-shaped surface.

may also help explain the above-mentioned 12 older samples. The similarity in surface exposure ages might be the result of exposure of the cobbles in the drainage basin, which is larger than those of the other sites. However, unless all cobbles

inherited essentially the same inventory of radionuclide we would predict that inheritance would most likely result in a greater age spread for each surface. Our results indicate a good coherence in age of all cobbles from each surface. We therefore

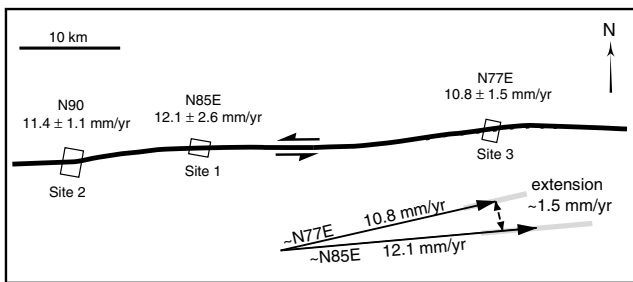


**Figure 14.** Slip-rates and fault strikes at three sites along Xidatan and Dongdatan. Slip-rate variations along the fault could be due to a change in fault strike. At site 3, the  $\sim 4$  m high vertical scarp (Fig. 13c) could be explained by extension on a more northeast-striking strand. Triangular diagram implies  $1.5 \text{ mm yr}^{-1}$  of extension in a  $\text{N}135\text{--}140^\circ\text{E}$  direction. The normal component of slip on the main fault and normal faulting on both sides of the Xidatan–Dongdatan trough (Figure 5) probably account for  $1.5 \text{ mm yr}^{-1}$  of extension normal to the strike-slip fault.

conclude that the most reasonable scenario is that the exposure ages indeed reflect the final abandonment of the surfaces.

We thus relate the offsets of the T3-3/T3-2 and T3-2/T3-1 risers to the ages of T3-2 and T3-1 ( $68 \pm 5$  m in  $6043 \pm 553$  yr, and  $47 \pm 5$  m in  $4837 \pm 857$  yr, respectively). The corresponding slip-rate values ( $11.3 \pm 1.9$  and  $9.7 \pm 2.8 \text{ mm yr}^{-1}$ ) are consistent with one another, and constrain the Late Holocene left-slip-rate along the fault in Dongdatan to  $10.8 \pm 1.5 \text{ mm yr}^{-1}$ .

#### 4.1.3 Slip variations and mean slip-rate

The mean slip-rates obtained at the three Xidatan–Dongdatan sites ( $12.1 \pm 2.6 \text{ mm yr}^{-1}$  at site 1,  $11.4 \pm 1.1 \text{ mm yr}^{-1}$  at site 2, and  $10.8 \pm 1.5 \text{ mm yr}^{-1}$  at site 3, Fig. 14) are similar within error and yield an average, uniform rate of slip along this segment of the Kunlun Fault of  $11.6 \pm 0.8 \text{ mm yr}^{-1}$  (Fig. 15).

The small decrease in sinistral slip-rate ( $\sim 1.3 \text{ mm yr}^{-1}$ ) between sites 1 and 3 could reflect the change in fault strike (from  $\sim \text{N}85^\circ\text{E}$  to  $\sim \text{N}77^\circ\text{E}$ ) over a distance of  $\sim 30$  km (Fig. 14; e.g. Gaudemer *et al.* 1995b; Peltzer *et al.* 1988b), consistent with an increase in strike-perpendicular extension, and hence with the existence of the south-facing, normal scarp observed at site 3 (Fig. 13b). The lack of precise topographic constraints at site 3

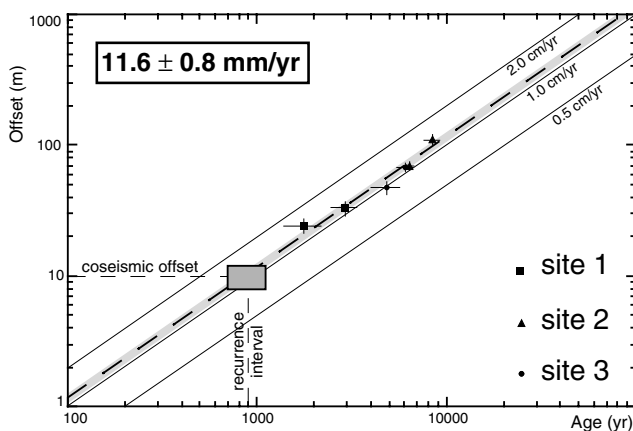


**Figure 15.** Mean Holocene left-slip-rate deduced from cosmogenic dating of alluvial terraces at three sites along Xidatan and Dongdatan. Coseismic offset (box) is deduced from the values in Table B5.

precludes accurate determination of the slip-vector, and the value of the second-order discrepancy discussed here is similar to the uncertainty on the horizontal slip-rate. Nevertheless, it is worth noting that the 4–4.6 m height of the scarp at site 3 would imply a vertical throw-rate of the order of  $\sim 0.8 \text{ mm yr}^{-1}$  in 5–6 kyr, corresponding to less than  $0.5 \text{ mm yr}^{-1}$  of extension across the fault if it dipped more than  $60^\circ$  SSE. The normal component of faulting across T3 would thus account for about one-third of the  $1.5 \text{ mm yr}^{-1}$  of strike-perpendicular extension that one might expect from the  $8^\circ$  northward bend in strike of the fault between the two sites (Fig. 14).

#### 4.1.4 Seismic behaviour of the fault in Xidatan–Dongdatan

When combined with additional geomorphic evidence of left-lateral displacement along the Xidatan–Dongdatan valley, the riser offsets and temporal emplacement sequence of the terraces at sites 1–3 shed light on the local seismic behaviour of the Kunlun Fault. Our data, with quantitative measurements and field observations, are best explained by the occurrence of infrequent, great earthquakes, as qualitatively inferred from the presence, and absence, of large mole tracks on high-, and low-level terraces, respectively. At six sites in Xidatan and at site 3 (Table 2), our tape measurements yield minimum sinistral

**Table 2.** Coseismic and cumulative offsets measured in the field along Xidatan and Dongdatan.

| Site          | marker type               | coseismic offset (m)         | cumulative offset (m)                  |                        |
|---------------|---------------------------|------------------------------|--|------------------------|
| Xidatan       | terrace riser             |                              | 18 ( $2 \times 9$ )                    |                        |
|               | channel                   |                              | 27 ( $3 \times 9$ )                    |                        |
|               | terrace riser             | 9.5                          |  |                        |
|               | stream                    | 12.5                         |  |                        |
|               | terrace riser             |                              | $29 \pm 3$ ( $3 \times 10$ )           |                        |
|               | fan edge                  |                              | $26$ ( $3 \times 9$ )                  |                        |
| site 2        | terrace riser             | 9                            |  |                        |
|               | stream                    | $9 \pm 0.5$                  |  |                        |
|               | terrace riser             |                              | $23 \pm 2$ ( $2 \times 12$ )           |                        |
|               | terrace riser             | $10.2 \pm 1$                 |  |                        |
|               | terrace riser             |                              | $110 \pm 10$                           |                        |
|               | terrace riser             |                              | $70 \pm 5$                             |                        |
| site 1        | terrace riser             | 9                            |  |                        |
|               | stream                    |                              | $29 \pm 1.5$ ( $3 \times 10$ )         |                        |
|               | terrace riser             | $24 \pm 3$ ( $2 \times 12$ ) |  |                        |
|               | terrace riser             | $33 \pm 4$ ( $3 \times 11$ ) |  |                        |
|               | gully                     | $50 \pm 5$                   |  |                        |
|               | Dongdatan                 | fan edge                     |  | $30$ ( $3 \times 10$ ) |
| terrace riser |                           |                              | $30$ ( $3 \times 10$ )                 |                        |
| stream        |                           |                              | $25$ ( $2 \times 12$ )                 |                        |
| stream        |                           |                              | $25$ ( $2 \times 12$ )                 |                        |
| site 3        |                           | terrace riser                | $8 \pm 1$                              |                        |
|               |                           | terrace riser                |  | $47 \pm 5$             |
|               | terrace riser             |                              | $68 \pm 5$                             |                        |
|               | fan edge                  |                              | $25$ ( $2 \times 12$ )                 |                        |
|               | stream                    |                              | $35$ ( $3 \times 12$ )                 |                        |
|               | terrace riser             |                              | $18$ ( $2 \times 9$ )                  |                        |
|               | gully                     |                              | $20$ ( $2 \times 10$ )                 |                        |
|               | gully                     |                              | $20$ ( $2 \times 10$ )                 |                        |
| stream        |                           | $25$ ( $2 \times 12$ )       |  |                        |
|               | Average coseismic offset: | $10 \pm 2$ m                 | Average coseismic offset: $10 \pm 2$ m |                        |

offsets of 8–12 m, compatible with those (10 m) found by Kidd & Molnar (1988) and Zhao (1996). At 18 sites in Xidatan and Dongdatan, we found cumulative horizontal offsets 2 or 3 times greater than 9, 10, 11 and 12 m (Table 2). Such least common denominator values, which vary by only 1 or 2 m from site-to-site, are thus likely to represent the coseismic surface-slip amounts of individual events breaking the fault. The dated cumulative offsets of  $24 \pm 3$  and  $33 \pm 4$  m at site 1, in particular, imply that two  $M \sim 8$  earthquakes, each with a displacement of 10–12 m, have offset the T2/T1 riser in the last  $\sim 1800$  yr, and that three such earthquakes are responsible for the offset of the T3/T2 riser in the last  $\sim 2900$  yr. In keeping with this interpretation, the  $\sim 50$  m gully channel offset on top of T3, and the very large sag-ponds and pressure ridges that deform that terrace surface (Figs 6a and 7a), might be the cumulative result of five comparably large earthquakes in the last  $\sim 5200$  yr. Results from trenching elsewhere in Xidatan (Zhao 1996) are compatible with the occurrence of four earthquakes in the last 4000 yr. The last event might have taken place prior to the  $280 \pm 89$  yr flash-flood on T1 at site 1, since no mole tracks are observed on this surface. Overall, the quantitative evidence at hand strongly suggests that the Xidatan–Dongdatan segment of the Kunlun Fault ruptures during great ( $M \sim 8$ ) earthquakes, with a characteristic slip  $\Delta u$  of  $\sim 10 \pm 2$  m and a recurrence time of  $\sim 900 \pm 200$  yr (Fig. 15).

## 4.2 Central, Dongxi Co segment

### 4.2.1 Tectonic and geological settings

The central, Dongxi Co–Anyemaqen segment of the Kunlun Fault strikes  $\sim N110$ – $130^\circ E$  between  $98^\circ E$  and  $99.5^\circ E$ , linking the more easterly striking Alag Hu and Maqen segments (Figs 2 and 16). In the east, the active fault trace veers along the base of the steep, northeastern front of the 40 km long Anyemaqen Shan range (Figs 16 and 17a). To the southwest, the Anyemaqen Shan is bounded by an active thrust fault, as well as the ranges west of it (Fig. 16 and C1). The strike-slip fault then continues for about 50 km northwestwards (Fig. C2), with a more uniform  $\sim N115$ – $120^\circ E$  trend. It subsequently crosses a large fluvial deltaic fan and swamps at the north-eastern corner of the Dongxi Co pull-apart lake (Fig. 16), before disappearing underwater along the northeastern shore of this lake. Two abandoned shorelines,  $\sim 3$  and 10 m above the lake, ring the eastern part of that shore. After a south-directed step or jog beneath the lake, the fault trace reappears at its southwestern corner, across lacustrine mud-flats and marshes, and continues westwards along a narrow topographic furrow. The surface break of the 1937 January 7,  $M = 7.5$ , earthquake (also named Tuosuohu earthquake), which is known to have ruptured this segment of the fault (e.g. Li & Jia 1981; Taponnier & Molnar 1977), is equally prominent and fresh west and east (Fig. 17b) of the lake and can be followed, with clear evidence of predominant left-lateral slip, all the way eastwards to the Qinglong river (Fig. 16).

Measurement of offset alluvial terraces, complemented by radiometric dating, was performed at two sites about halfway between the lake and the range, east of Huashixia (Fig. 16). Two north-flowing rivers from headwaters in the western Anyemaqen Shan cross the fault at these sites. South of the sites, the range is  $\sim 5000$  m in altitude, and ancient glacial

valleys upstream are currently ice-free, in contrast with the large glaciers that are fed by the 6000 m high Anyemaqen ice-cap only 40 km to the east. In keeping with this observation, this stretch of the fault, though  $\sim 4000$  m a.s.l. (Fig. 16), was apparently not crossed by ancient, now extinct, valley glaciers during the Last Glacial Maximum ( $\sim 20$  ka, e.g. Wang & Derbyshire 1987; Lehmkuhl *et al.* 1998), and hence we only mapped alluvial deposits in the vicinity of the fault trace at both sites.

The Anyemaqen range forms the leading, northern edge of the Songpan Garze terrane. It is chiefly composed of folded, Permian limestones intruded by basalts, and of Triassic flyschs, with low-grade metamorphism. A narrow belt of steeply dipping, probably Triassic, greenschists and slates, with schistosity roughly parallel to the fault, is exposed beneath Late Cenozoic deposits between the two sites. Cosmogenic-exposure dating could not be done at these sites because of the lack of datable samples. To constrain the ages of the terraces, we relied on  $^{14}C$  dating of fossil organic material and of charcoal fragments collected beneath shallow, alluvial or colluvial gravel, with loess or soil layers on top of them.

To determine horizontal and vertical offsets, we measured 28 and 22 topographic profiles at the first and second sites, from two and one bases, respectively. The profiles were levelled across the terraces and their risers, transverse and parallel to the fault trace, using a total station (digital-recording, infrared-laser, theodolite-distancemeter Wild T2000, DI3000). The levelling technique and associated measurement errors are discussed in Peltzer *et al.* (1988b), Avouac *et al.* (1993) and Gaudemer *et al.* (1995b). Given the intrinsic precision of the instrument and the size of the area surveyed, uncertainties in the offset measurements chiefly result from the definition of the geomorphic markers in the field.

### 4.2.2 Nianzha He (NZH) site

The Nianzha river is a large tributary of the Qinglong He (Fig. 16). Where it crosses the Kunlun Fault (Fig. 18), which locally strikes  $\sim N125^\circ E$ , the river has incised into several terraces, both upstream and downstream from the fault trace. The highest terraces are preserved on the left bank of the river. Most of them cap a flat,  $\sim 800$  m wide ledge cut into generally south-dipping Plio-Quaternary conglomerates, south of the fault. Along the base of the river-cut cliff that limits this ledge to the southwest, the  $\sim 600$  m broad Nianzha He flood-plain makes a  $\sim 3$  km long, SE-directed dogleg also parallel to the fault (Fig. 18). The high terrace ledge appears to be aligned with the hinge of a  $N120$ – $125^\circ E$ -trending, north-facing Quaternary anticline that forms an elongated hill south of the fault towards the northwest (push-up fold on Fig. 18a). We thus infer that the kink in the river course and the preservation of the peculiar, high terrace ledge result from ongoing, transpressional folding roughly parallel to the fault.

There are three main levels, T0, T1 and T2, each with several sublevels, numbered according to their increasing height and age (Fig. 18, C3 and C4, Table B1). T0 and T0' are the most recently abandoned sublevels, up to 6.3 m above the present-day river bed (Fig. 19). The four sublevels T1, T1', T1'' and T1''' together form the high terrace ledge between the fault and the river. They stand 30–40 m above the river where crossed by the fault (Fig. 19). Farther westwards, T2 is the highest

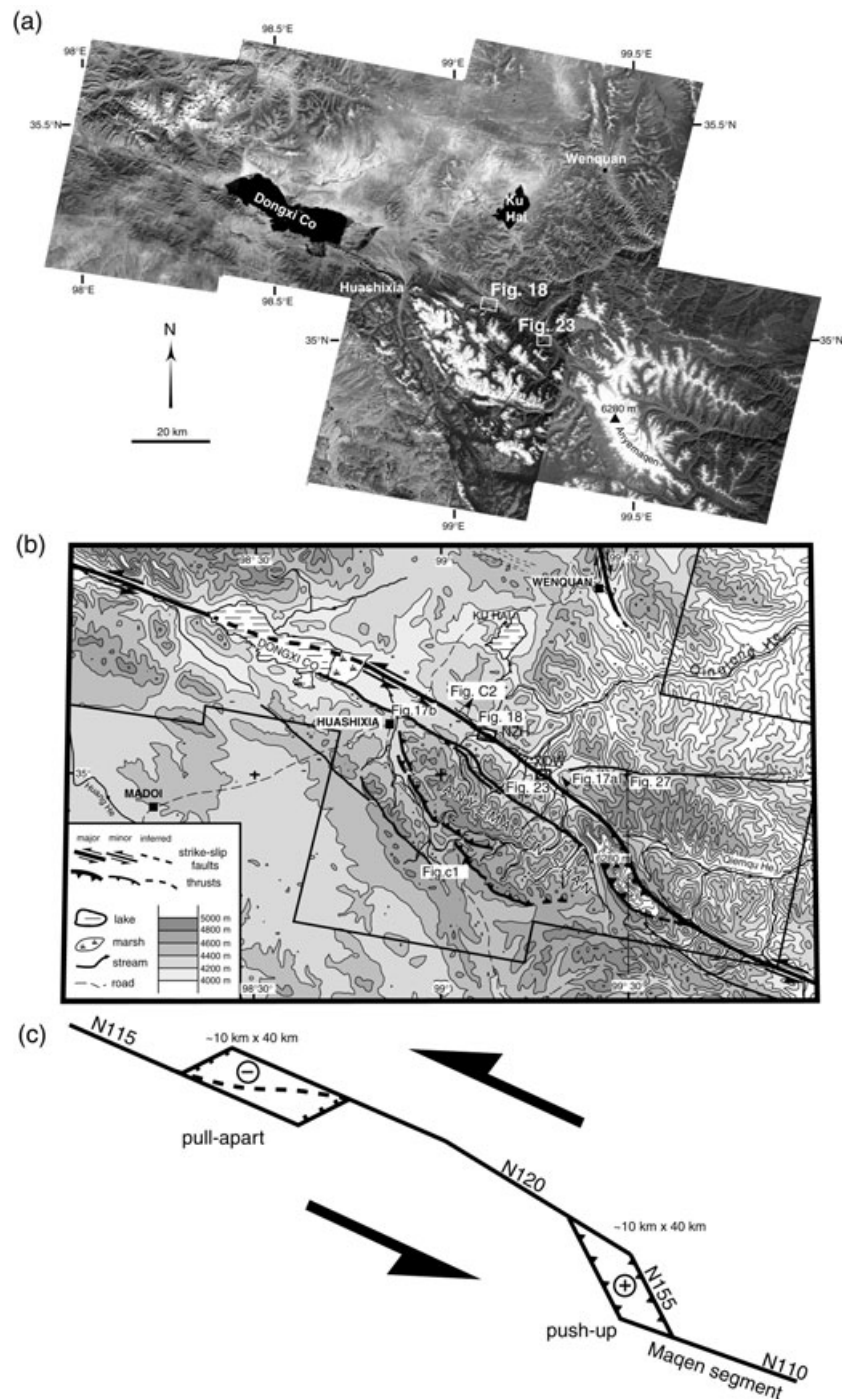


**Figure 16.** (a) SPOT satellite image mosaic of Dongxi Co segment. The N115°E-trending fault enters at the southwest corner and comes out at the northeast corner of Dongxi Co pull-apart lake. The highest summits of Anyemaqen (~6000 m a.s.l.) form a 40 km long crest line at the eastern end of the segment in a restraining bend of the fault. Boxes indicate the locations of Nian Zha He (Fig. 18) and Xiadawu sites (Fig. 23). (b) Tectonic map of Dongxi Co segment. The active strike-slip fault and thrust traces are from SPOT image interpretation and field work. Boxes indicate site locations and corresponding figures. (c) Schematic interpretation of left-lateral strike-slip fault geometry. The left step (west) and right step (east) have resulted in the Dongxi pull-apart and Anyemaqen push-up formations, respectively. These ~10 km wide and ~40 km long structures are probably of crustal scale.

fluvial terrace, more than 70 m above the river. It is possible to correlate the three main levels here with those found at the other site to the southeast.

The fault trace is marked by a northeast-facing scarp whose height increases with terrace elevation and age (Fig. 19), reflecting a small thrust component of slip related to strike-perpendicular shortening. The upper slope-break on T1 is

cut by the mole tracks of the 1937 earthquake. The position and shape of that scarp are consistent with north-vergent fold growth, which is in turn compatible with the south dip of the Quaternary beds beneath the terrace ledge. The steep, ~20 m high cut of the T1/T0 riser across the fault exposes greyish carbonatic gouge with shear planes dipping steeply south (N125±2°E, 85°S), in keeping with a component of

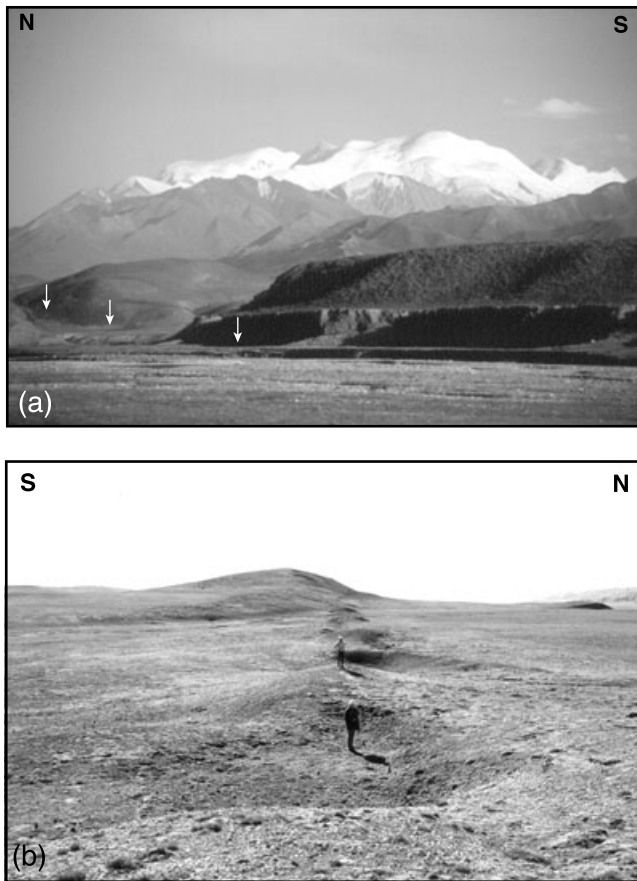


**Figure 17.** (a) View, looking east, of the ice- and snow-capped Anyemaqen peak (6280 m a.s.l.). The left-lateral Kunlun Fault (arrows) is in the foreground. (b) View, looking west, of 1937,  $M = 7.5$  earthquake mole tracks west of the Wenquan–Huashixia road.

reverse faulting. Some slickensides on comparable planes, however, have a small pitch to the southeast ( $\sim 12^\circ$ ), possibly related to extensional, near-surface faulting, as observed along the seismic mole tracks. Taking the drainage direction to be  $\sim N72^\circ E$ , parallel to the mean trend of the risers near the fault (Fig. 18c), and the corresponding steepest drainage gradient to be the average slope of riser profiles p03 and p24 ( $\sim 0.8^\circ$ , Fig. 19c), the apparent vertical throw due to horizontal slip would be only 0.85 per cent of the sinistral displacement, and hence at most about 9 per cent of the total vertical throw (Tables B1 and B2). Therefore, most of the vertical throw is due to perpendicular shortening, and only a small fraction results from the fact that the terraces do not slope perpendicularly to the fault (e.g. Gaudemer *et al.* 1995b).

The long profiles levelled west of the Nianzha river yield values of the vertical and horizontal offsets of the terrace risers (Fig. 19a, Table B2). The lowest riser ( $T0'/T0$ ), next to the river, is offset 4.1–4.4 m horizontally and 0.4 m vertically (p9, p10; Figs 19a and d, Table B2). Only a lower bound of the  $T1'/T0'$  offset ( $\sim 11.3 \pm 0.5$  m) can be estimated due to a small meander carved by the river and degraded further by regressive erosion, just upstream from the fault (Fig. 18, and p3 in Fig. 19a). The clearest horizontal offset ( $57 \pm 2$  m) is that of the  $T1'/T1$  riser (p24, Fig. 19a, Table B2). This riser is about 2 m high north of the fault, and almost twice as high (3.5 m) south of it (p4, p5, p6, p25, and p26, Fig. 19e), implying dip-slip

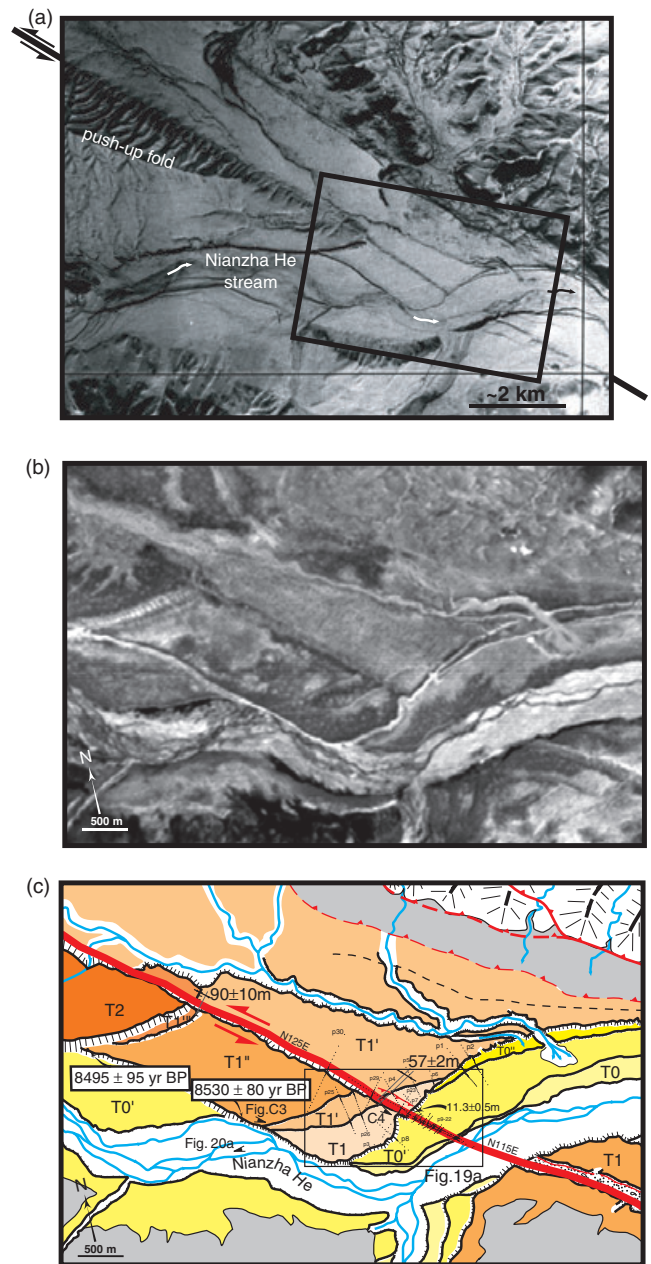


**Figure 18.** (a) Enlargement of an air photo of Nianzha He (NZH) site. Box indicates the location of (b). Scale is approximate. (b) Enlargement of SPOT image KJ248-280 of NZH site. The fault trace is marked by a straight, northeast-facing scarp across abandoned terraces on the left bank of Nianzha He. (c) Geomorphic interpretation of NZH site. Black dotted lines are topographic profiles levelled in the field. Radiocarbon ages and locations of samples are indicated.

movement on the fault while  $T1$  was the active flood plain. If one assumes that  $T1'/T1$  became a passive offset marker when  $T1$  was abandoned, then its horizontal offset and the vertical offset across  $T1$  ( $6.5 \pm 0.1$  m, p23, Fig. 19d, Table B2) accrued during the same time-span (see also case 5 of Fig. 4). The 2–3 m high  $T1''/T1'$  riser south of the fault (p25 and p26, Fig. 19e) has no counterpart north of it. The vertical offset of  $T1'$  is  $8.5 \pm 0.2$  m (p29, Fig. 19d, Table B2). Farther west, along the base of the colluvial slope separating  $T2$  from the  $T1$  ledge, a riser between a narrow terrace sublevel  $T1'''$  and  $T1''$  (Fig. 18)

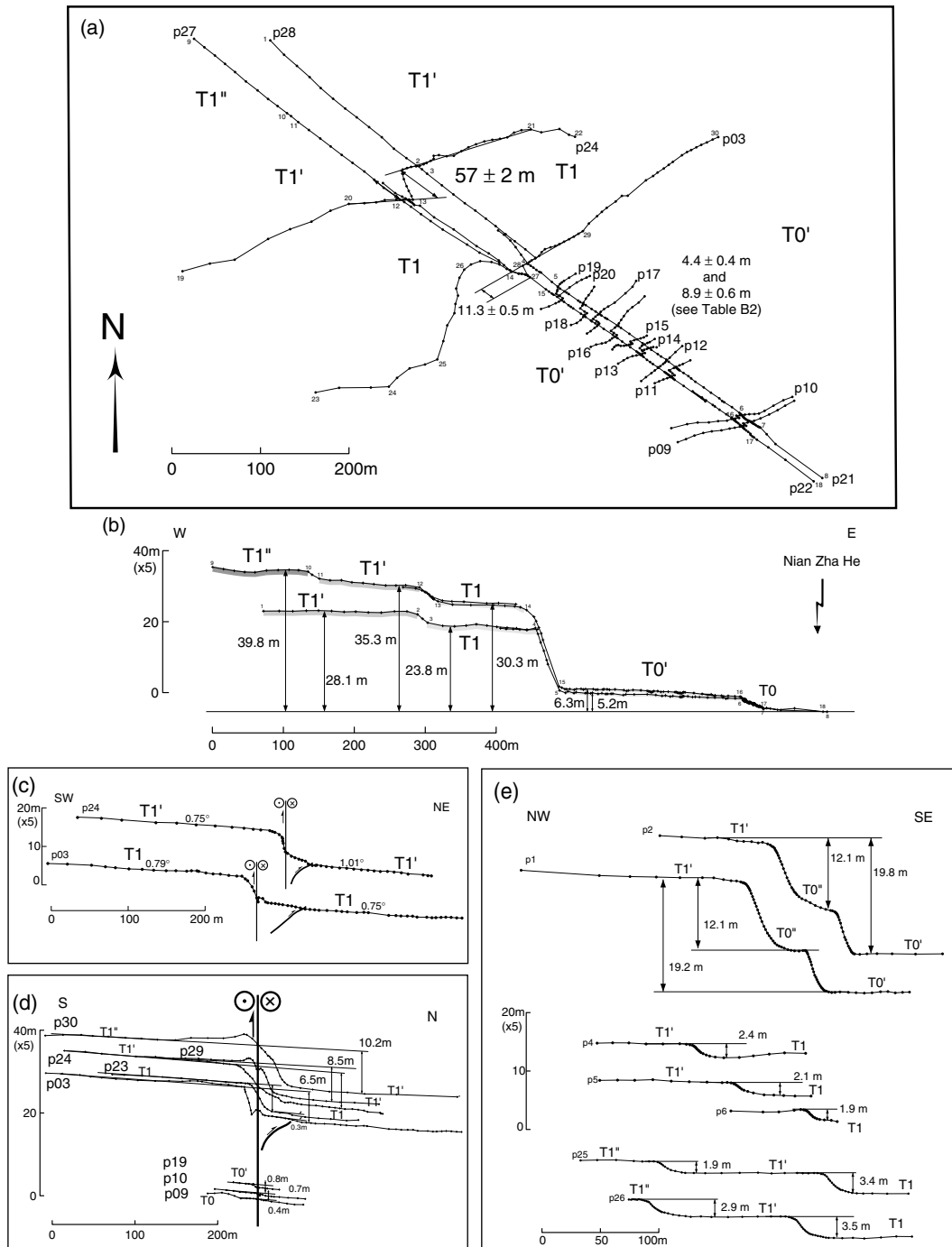


**Figure 19.** (a) Map view of profiles levelled in the field (see location in Fig. 22c). The left-lateral offset of the T1'/T1 riser is measured along 1937 earthquake mole tracks. (b) Projection of profiles p21, p22, p27 and p28 along the N125°E fault strike showing the cumulative vertical offset of terraces. (c) Projection of profiles p03 and p24 along the mean riser N60°E direction. Mean riser slopes are indicated. (d) Topographic profiles projected on the N35°E plane, orthogonal to the fault trace, and relative vertical offsets. (e) Topographic profiles, projected on N155°E (top) and N165°E (bottom) planes, orthogonal to terrace risers, and relative heights of terraces.

is offset by the fault. This sinistral offset, which was measured directly on the SPOT image, amounts to  $90 \pm 10$  m (Fig. 18c). Since the T1''/T1' riser does not exist north of the fault, the lower terrace at the base of T1'' north of the scarp may be T1' (Fig. 18). The vertical offset of T1''/T1'-T1' riser is thus at most that between T1'' and T1' ( $10.2 \pm 0.2$  m, p30, Fig. 19d, Table B2).

The sublevels on the T1 ledge are primarily made of loosely consolidated pebbles with additional fine gravel and sand. Together they form a conglomerate layer a few metres thick. The strath unconformity of T1' and T1'' on top of the south-dipping Plio-Quaternary beds is particularly well exposed along the south cliff of the ledge (Fig. 20a). The conglomerate is usually covered by a  $\sim 20$ – $40$  cm thick loess-rich soil layer, and

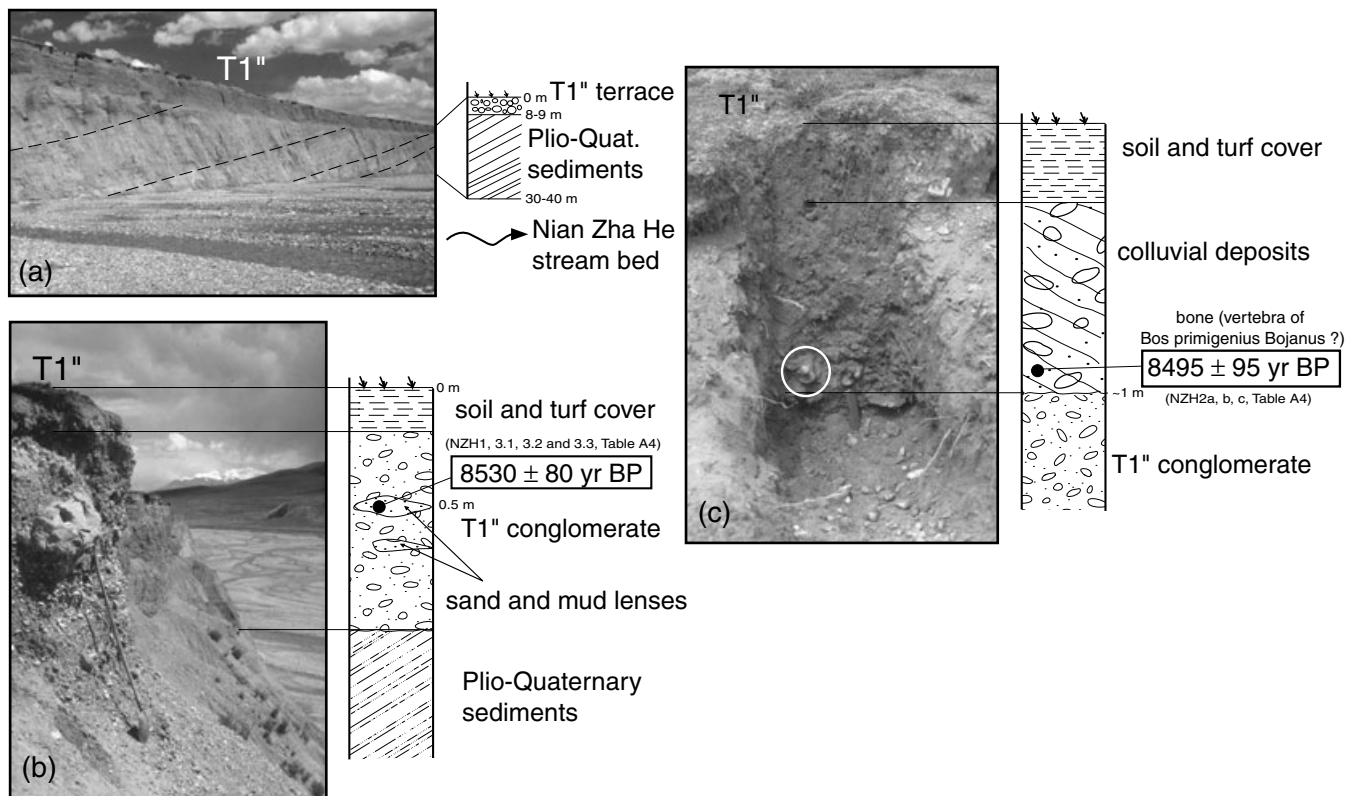


**Figure 20.** (a) View, towards the northeast, of T1'' strath terrace conglomerates, lying unconformably on top of SW-dipping, Plio-Quaternary sediments. The active stream bed is in the foreground. (b) Section of T1'' terrace and  $^{14}\text{C}$  sampling site. Small charcoal pieces were collected in sand and mud lenses within pebbly conglomerates approximately 0.5 m below the terrace top. (c) Bone (sample NZH2) found on top of pebbles belonging to T1'' terrace near the base of the T2/T1'' riser, about 0.6 m below the surface of the corresponding colluvial slope deposits.

by turf. On T1'' we collected charcoal fragments in a muddy sand lens, ~1.5–2 m deep, within the conglomerate layer, near the top of the ledge cliff (Fig. 20b). Three charcoal samples yielded calibrated  $^{14}\text{C}$  ages of  $8530 \pm 120$  a,  $8480 \pm 120$  a and  $8725 \pm 275$  a, with a mean of  $8530 \pm 80$  a (Table A4). Freshwater snail shells from the same sand lens provided an older age ( $9975 \pm 275$  a, Table A4). We also found a fossil bone (a vertebra of *Bos primigenius Bojanus*?) amongst the uppermost pebbles of T1'', in a 1 m deep pit dug beneath colluvium at the base of the T2/T1'' riser. This bone provided an age of  $8495 \pm 95$  a (Fig. 20c), consistent with the ages obtained for the same terrace about 1.8 km southeastwards. These  $^{14}\text{C}$  ages constrain the timing of the abandonment of T1'', which is the principal terrace sublevel on the high ledge, to post-date slightly  $8530 \pm 80$  a (Table A4). This early Holocene date is the only one we were able to obtain at this site.

The radiometric age of T1'' may be used to constrain the horizontal slip-rate. Since T1'' was abandoned after  $8530 \pm 80$  yr BP, the  $90 \pm 10$  m offset of the T1''/T1'' riser yields a minimum slip-rate of  $10.6 \pm 1.3$  mm yr $^{-1}$ . Although this riser may not be strictly coeval on either side of the scarp, it is also least likely to have been modified after 8500 yr BP north of the fault, given the sinistral sense of slip. The  $57 \pm 2$  m offset of the T1'/T1 riser must have accrued after the abandonment of T1, and thus after that of T1'' ( $8530 \pm 80$  yr BP). Hence, the slip-rate must thus be strictly greater than  $6.7$  mm yr $^{-1}$ . The age of T1 is not known, but may be estimated from the ratio between the vertical and horizontal offsets of the terraces across the fault, assuming this ratio to have been constant in the last few thousand years

(e.g. Gaudemer *et al.* 1995b). For T1, the ratio is  $8.8 \pm 0.4$ . For the coseismic offsets of the two comparable events found on T0', the mean value of that ratio is less well constrained and slightly greater ( $11.1 \pm 3.5$ ), possibly because the fault starts to veer northwards, by a few degrees, across T0'. Using the average value of these two ratios ( $9.9 \pm 2.3$ ) for all the high terrace sublevels (T1, T1', T1'' and T1''') would imply horizontal offsets of the T1''/T1' and T1'''/T1'' risers of  $84 \pm 20$  m and of less than  $101 \pm 25$  m, respectively. Given the age of T1'', the age of T1 should thus be less than  $5600 \pm 2245$  yr BP, and the sinistral slip-rate on the fault at the Nianzha He site greater than  $10.3 + 7.5 / - 2.9$  mm yr $^{-1}$ , consistent with the values estimated above.

In order to determine precisely the offset of the 1937 January 7,  $M=7.5$  earthquake, we levelled shorter profiles (Fig. 19a, Table B2) along offset rills that incise the lower terrace T0' (Fig. 21). These rill profiles show two distinct, statistically different groups of horizontal and vertical offset values, each with  $\Delta h \approx 11 \Delta v$ , corresponding to two earthquakes ( $\Delta h = 4.4 \pm 0.4$  m and  $\Delta v = 0.4 \pm 0.1$  m;  $\Delta h = 8.9 \pm 0.6$  m and  $\Delta v = 0.8 \pm 0.2$  m, for horizontal and vertical offsets, respectively; Table B2). The rills thus seem to have different ages and to have recorded the last (1937) and penultimate earthquakes on the fault. This inference is supported by the observation that the T0'/T0 riser top and base are offset by only 4.3 and 0.4 m (p9, p10, Figs 19a and d, Table B2). These offset values on T0' indicate that the last two earthquakes that ruptured the fault across the Nianzha He valley were very similar. The 11.3 m minimum offset of the degraded T1/T0' riser may be taken to record

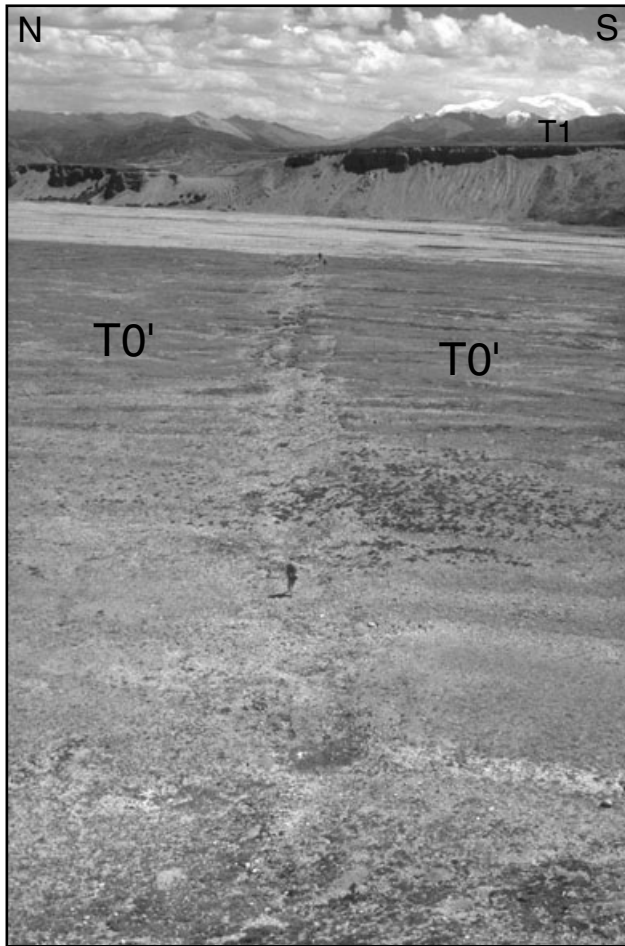


Figure 21. View, looking east, from T1 terrace, of T0' terrace. 1937 and subsequent earthquakes have offset small incised channels by about 8 m left-laterally and by 0.8 m vertically.

one more similar earthquake ( $3 \times 4.4 = 13.2$  m). As in Xidatan, this can be interpreted to indicate the occurrence of earthquakes of  $M \sim 7.5$  with characteristic slip of  $\Delta h \sim 4.4 \pm 0.4$  m and  $\Delta v \sim 0.4 \pm 0.1$  m on the Dongxi Co segment at Nianzha He. With a slip-rate of  $\sim 10.3 \text{ mm yr}^{-1}$ , the recurrence time ( $T_r$ ) of events comparable to the 1937 earthquake should be of the order of 420 yr (Fig. 22), with previous events in about  $1515 \pm 70$  AD and  $1095 \pm 140$  AD, and the next one due to occur in  $2350 \pm 70$  AD.

#### 4.2.3 Xiadawu (XDW) site

The second site along the Dongxi segment is located about 20 km southeastwards of the Nianzha He, on another tributary of the Qinglong He (Fig. 16). Three main terrace levels, T0, T1 and T2, are also observed here (Figs 23 and 24), implying an abandonment and an incision history comparable to that observed in the Nianzha He valley, even though the Xiadawu river is smaller (Fig. 16). The N125°E-striking Kunlun Fault trace is outlined by the straight road that follows the fault and crosses the village of Xiadawu built on terrace T1 (Figs 23 and 24).

The relative elevations and slopes of the terraces, as well as the shapes, heights and trends of the risers are constrained by the total station profiles (Figs 23c and 25, Table B3). The main

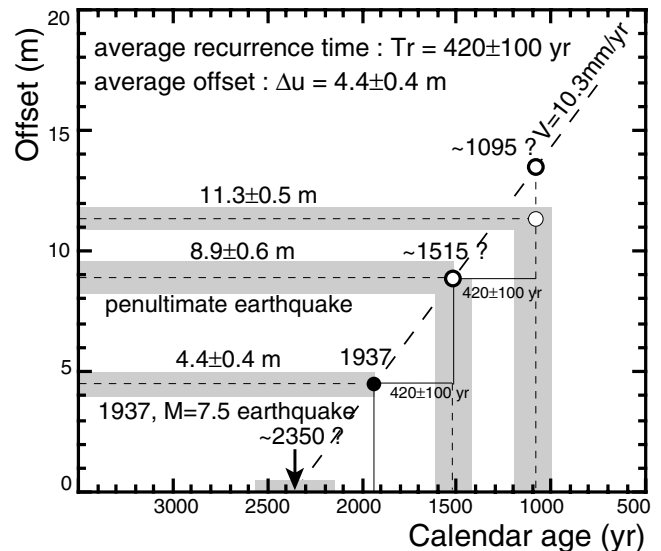
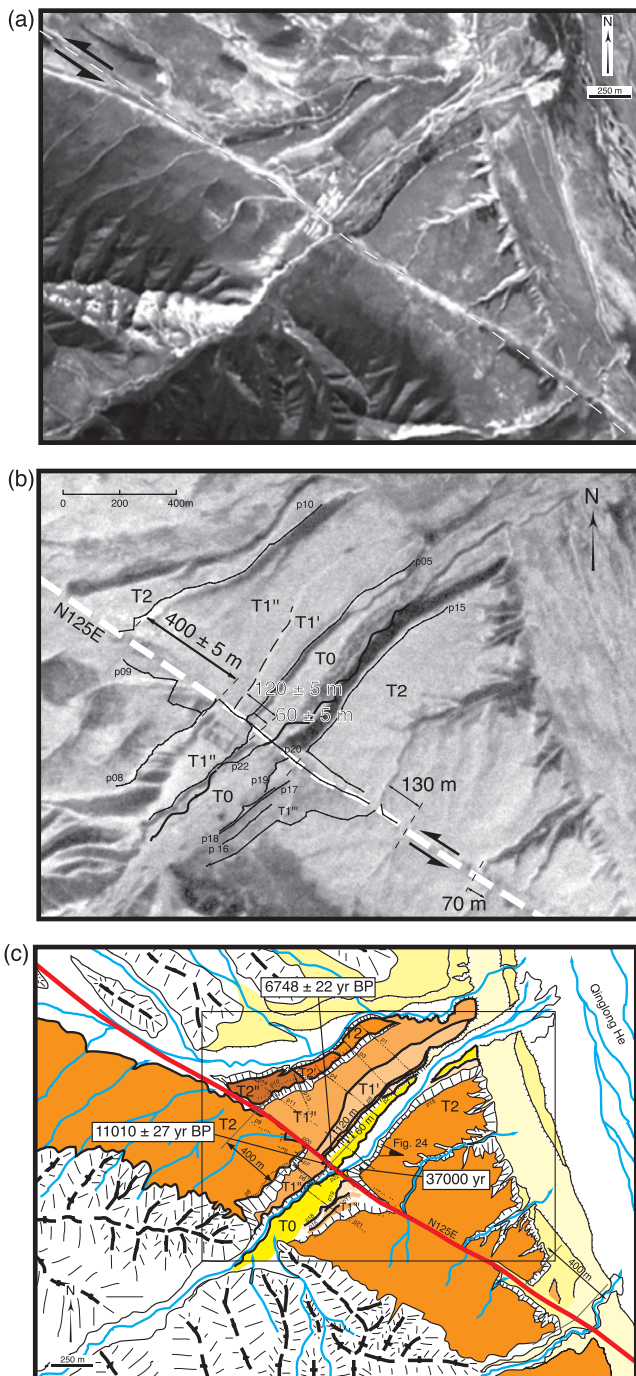


Figure 22. Plausible recurrence time and dates of previous large earthquakes comparable to the 1937,  $M=7.5$ , earthquake, based on offset measurements and the mean slip-rate determined at NZH site.

treads of terrace T2 stand 37–40 m above the Xiadawu riverbed (p1–p4, p8, p15, p21, Fig. 25, Table B3), except for one sub-level of that terrace, to the west, north of the fault (T2''), which is up to 55 m above the river (p11 and p10, Figs 25a and c). The principal sublevels of the T1 terrace surface (T1', T1'') stand 13–19 m above the river (Fig. 25, Table B3). One additional, narrow terrace ledge (T1''') on the right bank of the river south of the fault lies  $\sim 25$  m above the riverbed (p16, Fig. 25b). On the left bank north of the fault, the lowest, most recently abandoned terrace surface, T0, is 2–3.7 m above water (p3, p4 and p11, Fig. 25a). Two cliffs, one upstream from the fault on the left bank, the other downstream on the right bank, in which lateral cutting by the river has exposed the T1 and T2 main terraces in section, show that they are different from those in the Nianzha He valley. Here, T1 and T2 were emplaced as thick conglomeratic fills rather than as strath terraces (Figs A3, A4 and A5). The left-bank cliff also exposes folding of steeply north-dipping Plio-Quaternary sandstone and conglomerate beds, mostly beneath T2 and upstream from a near-vertical fault south of the active fault. Bedding slip may offset the surface of the north-sloping mountain flank above this north-facing, Plio-Quaternary anticlinal limb, but there is no measurable vertical throw across the main strike-slip fault (p15, Fig. 25b; p5, Fig. 25c).

The two highest risers west of the river (T2/T1 and T1/T0) are sinistrally offset across the fault by about 400 and 60 m, respectively (Fig. 23c). Restoring by these amounts the region south of the fault relative to the north (Fig. B1) yields good fits to other offsets east of the river. The continuity of the two risers—both displaced by  $\sim 400$  m—that bound the trapezoidal prong capped by T2 between the Xiadawu and Qinglong rivers, for instance, is restored. 400 m of back-slip also realigns the high risers that limit the western edge of the former floodplain of the Qinglong river north and south of the fault. West of Xiadawu, the  $\sim 30$  m high T2/T1'' riser is particularly well preserved. North of the fault, it was protected from river action due to sinistral slip. To the south, it became distinct from the T1''/T0 riser due to the eastward shift of the river incision



**Figure 23.** (a) Enlargement of SPOT image KJ248-280 of Xiadawu (XDW) site. (b) Air photo of XDW site. Black lines are topographic profiles levelled in the field along terrace risers. Note the 120 m left-lateral offset of the flat channel, north of the fault, on the left-bank terrace of the main stream. (c) Geomorphic interpretation of XDW site. Dated deposits on T1 and T2, and corresponding ages, are indicated. The rectangle corresponds to part (b).

into T1''. The dogleg offset of this riser, which is nearly orthogonal to the fault, can thus be accurately measured ( $400 \pm 5$  m; p10, p8, Figs 23b and c). The riser bounding T2 east of the river is less well defined. North of the fault, it coincides with the 38 m high T2/T0 cliff presently refreshed by river cutting. To the south, it is marked by the arcuate, gentle slope-break

between T2 and T1'', which meets the fault trace at a low angle (Figs 23b and c). The restored offset of that riser, however, is also close to 400 m (Fig. B1).

Smaller offsets have been recorded by the younger terraces T1'' and T1' west of the Xiadawu river. South of the fault, T1'' forms a small triangular ledge which widens northwards between the T2/T1'' and T1''/T0 risers (p6, p7, p9, Figs 23 and 25a). North of the fault, the same terrace sublevel covers a broader area (p11, Figs 23 and 25a) and is incised by a flat-floored, ~30–100 m wide, ~1.4–2.6 m deep channel (T1') clearly visible on the air photos (Fig. 23b). The eastern edge of this shallow channel, which is nearly orthogonal to the fault, follows closely the T1''/T0 riser, isolating a narrow T1'' tongue (p1, p3, p4, p11, Figs 25a and 26). The western edge of the channel (east-facing T1''/T1' riser) is sinistrally offset by  $120 \pm 5$  m relative to the T1''/T0 riser south of the fault (Fig. 23b). In turn, the T1''/T0 riser north of the fault is sinistrally offset by  $60 \pm 5$  m relative to its position south of the fault (Fig. 23). Both values should be considered minimum offsets since the T1''/T0 riser south of the fault is not a fossil riser but a cliff refreshed by river cutting along its base (Fig. A4).

We retrieved, and dated with  $^{14}\text{C}$ , a total of 12 charcoal samples, as well as one bone fragment, and small snail shells from beneath the T1'' and T2 terrace surfaces (Table A5). West of the river, in the loess-rich palaeosol immediately above the gravels topping the narrow tongue of T1'' fill north of the fault, 8 charcoal fragments yielded a mean calibrated age of  $6748 \pm 22$  yr BP (Figs 23c, 26 and A3, Table A5). This age probably predates the deep incision of the river east of the T1'' tongue and the formation of the T1''/T0 riser. Four other charcoal samples collected south of the fault on the same side of the river, within the uppermost fanglomerates of the T1'' fill, below a 1 m thick loess layer, yielded a mean calibrated age of  $11\,010 \pm 27$  yr BP, while one bone at the same location yielded a younger date ( $10\,477 \pm 101$  yr BP, Figs 23c, 26 and A4; Table A5). These latter samples must slightly predate the final emplacement of T1'' and the subsequent deposition of T1' into the shallow channel north of the fault. The freshwater snail shells collected in the uppermost part of the T2/T0 riser cliff, just north of the fault on the right bank of the river, in a mud and sand horizon about 3 m below the surface of the T2 terrace, yielded an uncalibrated age of about 37 000 yr (Figs 23c and A5, Table A5). This value is a maximum age for T2, since pebble layers overlie the shell rich horizon.

The ages of T1'' north and south of the fault, and of T2 north of the fault represent maximum ages for the offsets of risers T1''/T0, T1''/T1' and T2/T1'', respectively. Moreover, because both T1'' and T2 are fill rather than strath terraces, the T2/T1'' and T1''/T0 risers are unlikely to be coeval with the abandonment of T1'' and T0, respectively. Therefore, the offsets and ages measured at Xiadawu provide lower limits for the sinistral slip-rate on the fault. The  $120 \pm 5$  m offset must have been recorded since the final emplacement of T1'', i.e. after  $11\,010 \pm 27$  yr BP. Similarly, the  $60 \pm 5$  m offset must have been recorded after T1' was completely abandoned, hence after  $6748 \pm 22$  yr BP. The maximum ages and minimum offsets west of the river yield compatible slip-rates of at least  $\sim 10$  mm yr $^{-1}$  ( $10.9 \pm 0.5$  and  $8.9 \pm 0.7$  mm yr $^{-1}$ , respectively). Finally, though not calibrated, the 37 000 yr age of T2 east of the river, which is a maximum age for the  $400 \pm 5$  m offset of the T2/T1'' riser, also yields a minimum slip-rate of 10.8 mm yr $^{-1}$ .

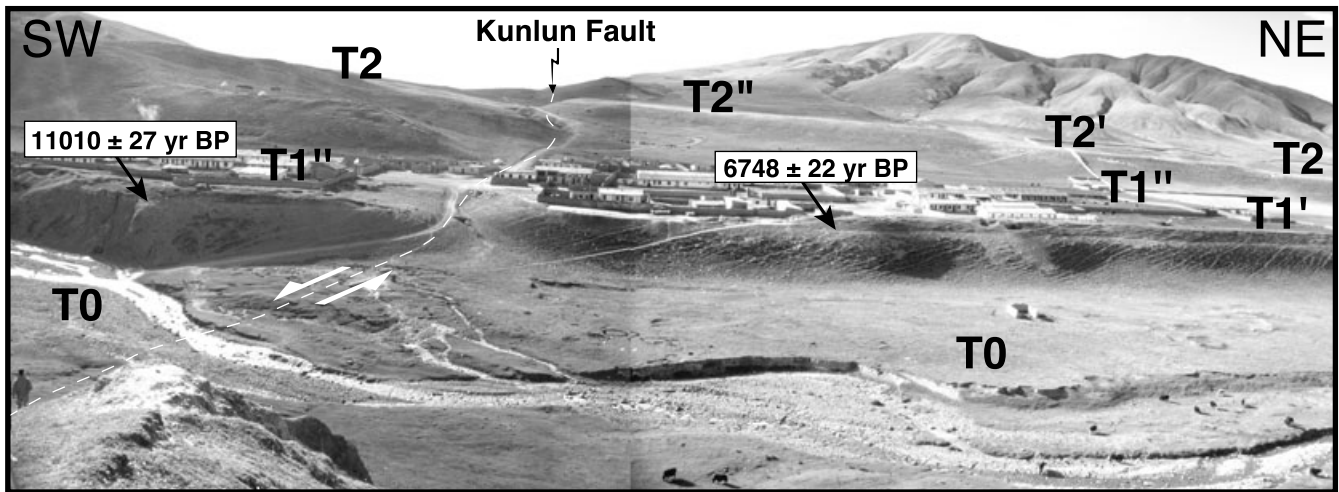


**Figure 24.** Panoramic, composite view of Xiadawu site. The village is built on either side of the fault, on various levels composing T1. The T1/T0 riser is offset by about 60 m; the T2/T1 riser, by 400 m.  $^{14}\text{C}$  ages of organic material found in terrace pebbles are indicated.

Taken together, our age measurements at Nianzha He and Xiadawu sites, only  $\sim 20$  km apart north of the western Anyemaqen range, imply a left-slip-rate slightly greater than  $1 \text{ cm yr}^{-1}$  on the Dongxi segment of the Kunlun Fault during at least the Holocene and probably the last 40 000 yr.

#### 4.3 Eastern Maqen segment

East of the highest peaks of the Anyemaqen range (Figs 2 and 16), the Maqen (or Dawu) segment of the fault resumes a  $\text{N}110^\circ\text{E}$  strike (Fig. 27). Here, the fault separates a belt of folded Permian limestones and marbles intruded by gabbroic/basaltic sills, with sheared harzburgite fault-slices, to the south, from a more monotonous zone of folded, low-grade Triassic slates, to the north. Unconformable Cretaceous–Palaeogene red-beds on either side of the fault are also folded. West of Maqen, two stretches of the fault are marked by prominent shutter ridges, whose incision by deviated streams exposes tens of metres of thick, black, clay-rich gouge zones with steeply dipping slices of various sheared rocks (ochre and red sandstones, limestones; Fig. 28). The largest streams flowing north across the fault display clear cumulative offsets of 4.1–12.8 km (Fig. 27b).

East of a small releasing bend near Maqen, the fault trace crosses high ground ( $\sim 4000$  m a.s.l.), where numerous sinistral offsets of late- to postglacial geomorphic features are preserved. We documented in greater detail one cumulative offset at Kending Na, about 30 km east of Maqen. The main strand of the fault here has cut and displaced the western, lateral moraine of a now-extinct, formerly south-flowing glacier (Figs 29 and B2). The two segments of the moraine north and south of the fault are cleanly truncated and disconnected, which implies that their offset post-dates complete withdrawal of the glacier across the fault. As measured either with a tape in the field or by restoration on the SPOT image, the moraine offset is  $180 \pm 20$  m. North of the fault, several inset terraces (T1, T2, T3; Fig. B2) have been abandoned by the formerly glacial outwash stream, as it was deviated and dammed by the growing sinistral offset of the moraine and of adjacent deposits.

Four charcoal samples were collected in pits dug into the highest terrace surface upstream from the fault (T3), and on the east side of each morainic ridge on either side of the fault.

The two samples on the ridges, C1 and C4, were retrieved at depths of 0.9 m and 0.5 m within thick, dark brown and black soil above a yellow, loess-rich layer. They yield relatively young  $^{14}\text{C}$  ages of  $4851 \pm 20$  and  $995 \pm 56$  yr BP, respectively (Table A6). One sample on T3 (C2), also within thick soil at a depth of 1 m, 10 cm above gravels, yields an intermediate  $^{14}\text{C}$  age of  $3546 \pm 77$  yr BP. The other sample on T3, which was found at a depth of 0.6 m, atop of gravels and beneath a loess layer, yields a much older  $^{14}\text{C}$  age of  $11\,156 \pm 157$  yr BP (Table A6). We take this age to be close to that of abandonment of T3. Both segments of the formerly continuous morainic ridge have fresh and well-preserved shapes, and boulders still protrude on their surfaces. The moraine thus appears to be young, probably due to the farthest advance onto the piedmont bajada during the Last Glacial Maximum (LGM  $\sim 20$  ka; e.g. Thompson *et al.* 1997). Furthermore, it must have been abandoned prior to the emplacement of T3  $\sim 11$  kyr ago. Hence, an age between 20 and 11 ka, and a cumulative offset of  $180 \pm 20$  m imply a slip-rate of  $12.5 \pm 2.5 \text{ mm yr}^{-1}$  on the fault, comparable to that found farther west.

Smaller offsets of low-level terrace risers and rills (Fig. 30) measured over a 20 km long stretch of the fault west of the offset-moraine site range between 12 and 36 m. That no offset smaller than 12 m was found is suggestive of great earthquakes. Combining the slip-rate estimated above and a minimum offset of 12 m per event, the recurrence time of earthquakes on the Maqen segment of the Kunlun Fault would thus be of the order of 1000 yr. The well-smoothed surface trace of the fault implies, however, that no such earthquake has occurred east of Anyemaqen Shan in the last few centuries.

## 5 DISCUSSION

### 5.1 Mean slip-rate along the Kunlun Fault

This study is the first to use  $^{26}\text{Al}$  and  $^{10}\text{Be}$  surface exposure dating in conjunction with  $^{14}\text{C}$  to quantify slip-rates along the Kunlun Fault. That  $^{14}\text{C}$  dates corroborate mutually consistent  $^{26}\text{Al}$  and  $^{10}\text{Be}$  model ages demonstrates that cosmogenic dating of fossil offset features on alluvial surfaces is a powerful tool for determining slip-rates on active faults, particularly at high elevation.

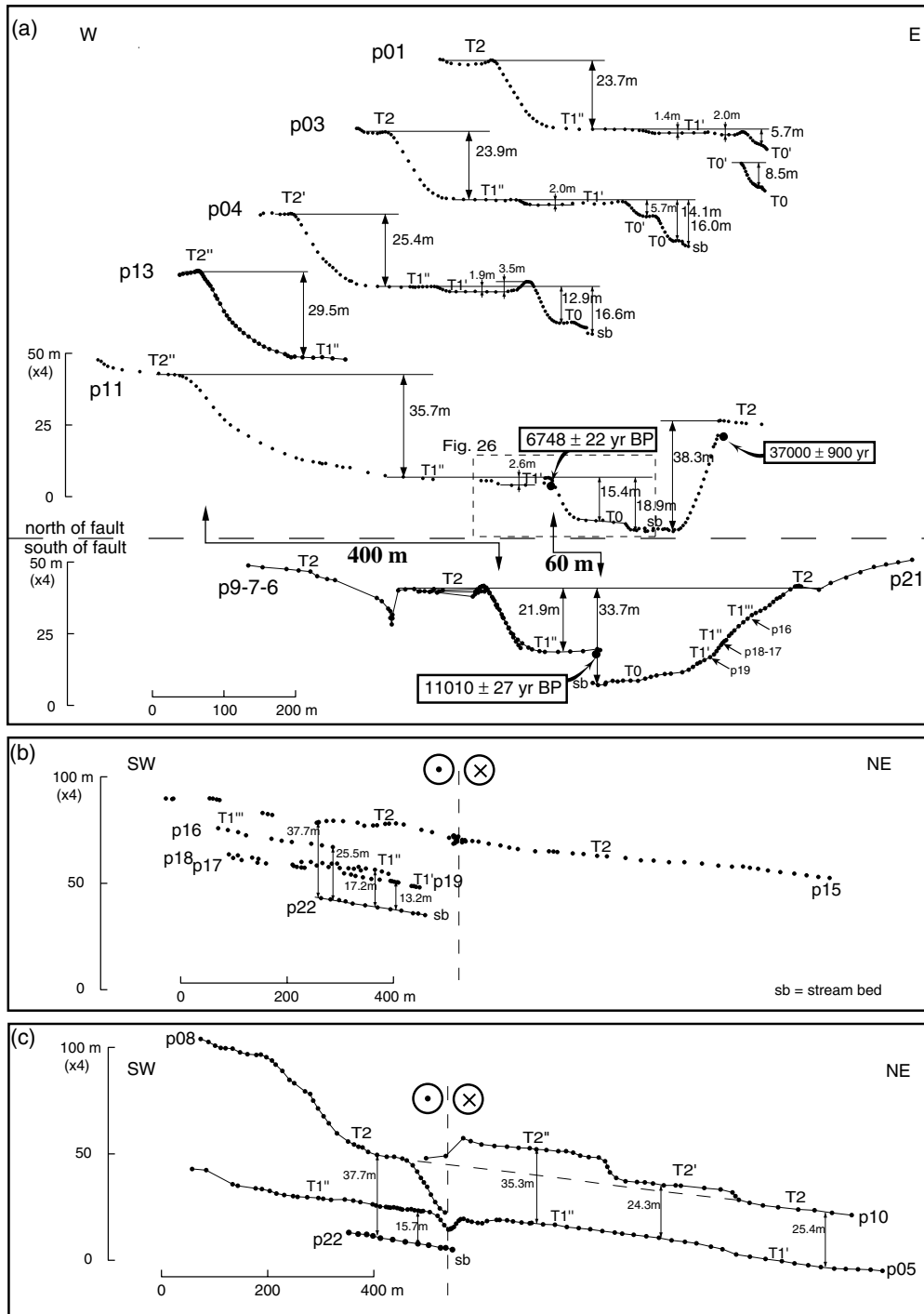


**Figure 25.** (a) Topographic profiles of terrace levels, projected on a N125°E-striking plane, parallel to the fault and transverse to the Xiadawu stream valley. Ages and heights of various levels are indicated. (b) Projection of terrace profiles on a N40°E-striking plane, parallel to the maximum slope and stream valley, and transverse to the fault on the east side of the stream. (c) As (b), for profiles on the west side of the stream.

The ages of the terraces in Xidatan–Dongdatan, like those of debris-flow fans in Owens Valley in California (Bierman *et al.* 1995), were determined from samples collected exclusively on their surfaces. In both cases, age determinations were facilitated by the proximity between the site of deposition and the source region, resulting in little inheritance (less than  $\sim 278 \pm 87$  yr at site 1). Although this simple sampling strategy was successful here, it should be used with caution and is not expected to be universally applicable to alluvial surfaces,

yielding erroneously high ages as pre-depositional exposure becomes more important (e.g. Brown *et al.* 1998). Larger sample sets, which may provide better average nuclide concentrations, will not by themselves solve this problem, as they are likely to represent the sum of both average, post-depositional exposure and average inheritance. In general, therefore, they should yield maximum ages, and ought to be coupled with additional, subsurface sampling that explicitly accounts for inheritance (e.g. Anderson *et al.* 1996; Repka *et al.* 1997).

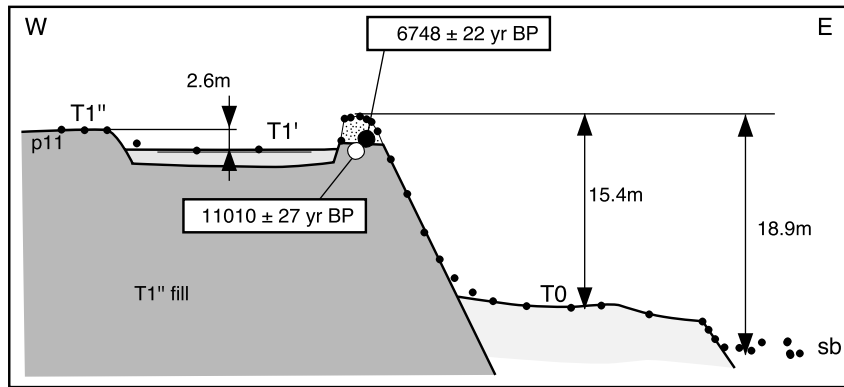


Figure 26. Schematic E-W cross-section of terraces and positions of charcoal samples at site XDW (see Fig. 25).

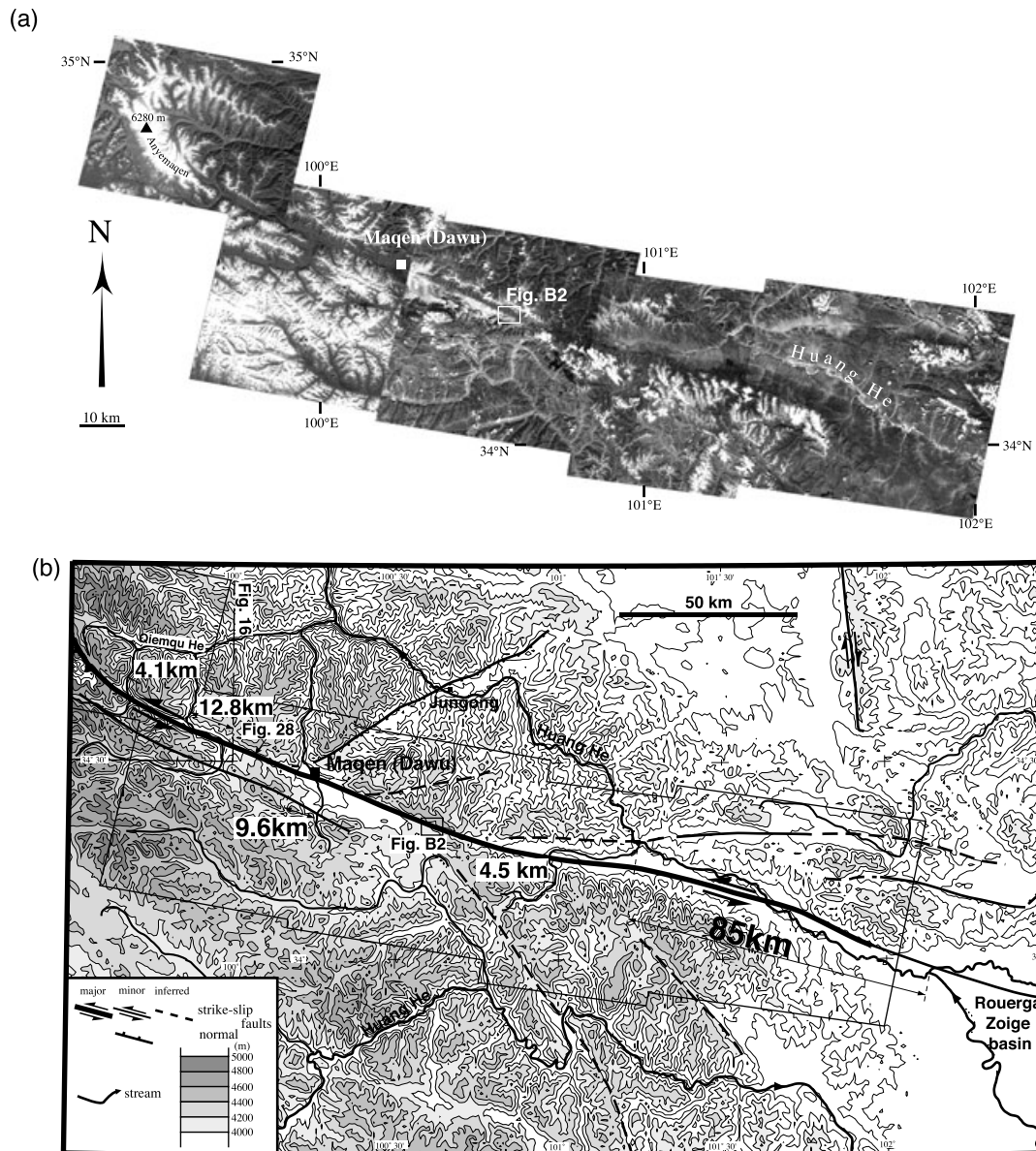
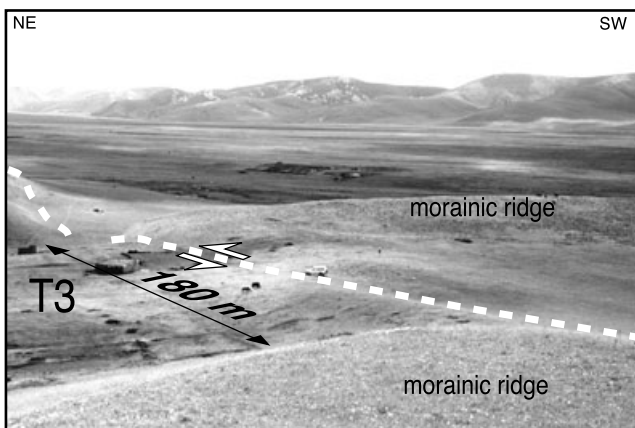


Figure 27. (a) SPOT image mosaic of Maqen segment. The fault strikes N110°E south of the narrow valley at the southwestern termination of Anyemaqen Shan. It then crosses the Maqen releasing bend and continues north of the valley for about 70 km. Towards the east, the fault enters a wide valley drained by Huang He. (b) Tectonic map of Maqen segment. Active fault traces are from SPOT image interpretation and field observations.



**Figure 28.** View, looking west, along fault strike of the shutter ridge west of Maqen (see Fig. 27b for location). The stream incision across the ridge reveals several tens of metres of thick, vertical gouge.



**Figure 29.** View of the offset LGM moraine ridge and T3 terrace level, abandoned after  $11\,156 \pm 157$  yr BP.

At six different sites we dated as many as 93 quartz pebbles and 22 organic samples to constrain the ages of the cumulative offsets of 11 distinct morphological markers. The large number of samples is paramount in obtaining statistically meaningful cosmogenic ages, and in identifying clearly and discarding outliers on any given terrace. Several independent values of



**Figure 30.** View, looking south, of a small gully offset by the Kunlun Fault. The offset, probably resulting from only one large earthquake, is about 12 m.

both the marker ages and slip-rates, based either on cosmogenic or  $^{14}\text{C}$  dating, are consistent with one another at each site and from site-to-site (Fig. 31), giving us confidence in individual rate determinations. Overall, our estimate of the slip-rate is determined within an uncertainty of  $\pm 2.0$  mm yr $^{-1}$ , and the average value of 11.5 mm yr $^{-1}$  is robust (Fig. 31).

For offset risers, the ages we take, and hence the slip-rates, depend on field interpretation regarding the terraces (strath in general, fill in one case), the nature of which may vary from site-to-site or at a given site. An end-member scenario, considered highly unlikely, is that the ages of all riser offsets are those of upper terraces. Slip-rates derived in this scenario are  $\sim 7$  mm yr $^{-1}$ . In view of geological evidence, we believe 7 mm yr $^{-1}$  to be implausibly small. Nonetheless, this value is greater than the rate inferred from two epoch remeasurements of the few extant GPS stations north and south of the Kunlun Fault (Chen *et al.* 2000). Until a denser and longer GPS survey is undertaken, slip-rates based on this technique should be regarded as preliminary.

Our average rate value of  $11.6 \pm 0.8$  mm yr $^{-1}$  in Xidatan–Dongdatan (Fig. 15), which is based only on cosmogenic dating of offset terrace risers, is consistent with those derived from other geological studies with different dating techniques. Zhao *et al.* (1994) and Zhao (1996), in particular, documented 10 offsets of gullies and terrace risers in Xidatan, ranging from 10 to 152 m, and retrieved seven TL or  $^{14}\text{C}$  ages, ranging from 2.14 to 12.0 kyr BP, with uncertainties of 6–9 per cent. From this, they derived a Holocene slip-rate of about 11.5 mm yr $^{-1}$ . Unfortunately, without error estimates on the offsets, the uncertainty on that rate cannot be assessed. The average Quaternary rate estimated by Kidd & Molnar (1988) (10–20 mm yr $^{-1}$ ), loosely brackets both our values and those of Zhao *et al.* In a strict sense, however, it cannot be simply compared with either, because it corresponds to a much longer time-span. Recall that the long-term rate of Kidd & Molnar (1988) is deduced from the separation between Lower Pleistocene moraines containing boulders of pyroxenite, south and east of the Kunlun Pass, and their presumed source area, 30 km to the west, in the mountains north of the fault. The factor of two in the estimate comes chiefly from the large uncertainty in the age of the lake-beds that overlie the moraine (2.8–1.5 Ma) (Kidd & Molnar 1988; Qian *et al.* 1982; Wu *et al.* 1982). To this uncertainty on the age, one should also probably add a  $\sim 30$  per cent error on the offset, due to poor definition of the eastern piercing point (Kidd & Molnar 1988: Fig. 6). Hence, while it is interesting to note that there is no first-order discrepancy between the loosely constrained, average Quaternary rate (Kidd & Molnar 1988) and the Holocene slip-rates derived from  $^{14}\text{C}$ , TL or cosmogenic dating, kinematic models of the current tectonics of northeast Tibet making use of the latter rates will be more precise.

## 5.2 Climatic origin of the morphology

Along the Xidatan–Dongdatan valleys, the relatively small number of terrace levels (about seven, Fig. 5) found along most of the streams implies a relatively uniform morphological response on a regional scale. It seems that most of the streams emplaced terraces at discrete, comparable times. Not all the streams deposited all the terrace levels identified, however. The variable distribution of terraces along the different streams is thus probably due to local conditions in each watershed.

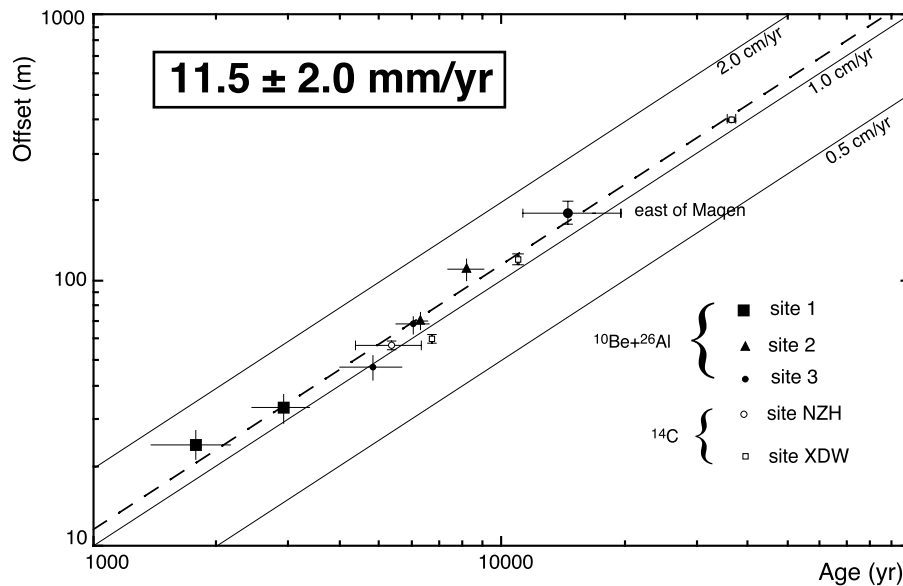


**Figure 31.** Summary of Holocene left-slip-rates deduced from cosmogenic and  $^{14}\text{C}$  dating of alluvial terraces at six sites along Kunlun Fault. The great consistency between independent values obtained with different dating techniques implies a uniform average slip-rate of  $11.5 \text{ mm yr}^{-1}$  along 600 km of fault.

In particular, the wedge-shaped Burhan Budai Shan, which is narrow in the west and widens towards the east, with decreasing elevation, leads to widening of drainage catchments towards the east, and steepening towards the west (Fig. 5a). Large glaciers cap the western part of the range south of Xidatan, while small glaciers fill the upper reaches of the long and narrow valleys south of Dongdatan (Fig. 5a). One might therefore expect distinct responses of the different drainages in terms of bed-load transport and stream power, and hence in terms of incision and terrace formation (Bull 1991). In spite of the differences in the watersheds, however, the relatively uniform pattern of terraces suggests a regional emplacement of chiefly climatic origin.

The  $^{26}\text{Al}$ ,  $^{10}\text{Be}$ , and  $^{14}\text{C}$  ages obtained here indicate that the majority of the morphological markers, for the most part alluvial terraces, were emplaced after the Last Glacial Maximum ( $\sim 20 \text{ ka}$ ; e.g. Bard *et al.* 1990; Thompson *et al.* 1997). Most of the ages range between 5 and 13 ka, post-dating the late-glacial warming at  $\sim 14.5 \text{ ka}$ , and bracketing the wettest period of the Early Holocene optimum (9–6 ka; e.g. Gasse *et al.* 1991; Yan *et al.* 1999). This is compatible with the occurrence of pollen in cores of the Dunde Ice Cap,  $\sim 300 \text{ km}$  to the northeast, suggesting that the summer monsoon extended into northeast Tibet during the first half of the Holocene (Liu *et al.* 1998), and that the subsequent climate was more arid with intervening humid periods (e.g. Gasse *et al.* 1991). The youngest terraces are probably related to such late Holocene pluvials (Liu *et al.* 1998). In general, therefore, terrace emplacement and incision appear to have been coeval with periods of fluctuating precipitation.

Only along the central, Dongxi segment of the fault did we find a well-preserved, alluvial surface older than the LGM ( $\sim 37 \text{ 000 yr}$ ). In Xidatan and Dongdatan, the ages of a few outliers in the sample population also appear to be related to pre-14.5 ka climatic events. Three such outliers (22.8 ka, site 1; 24.7 ka, site 2; 28.5 ka, site 3) probably correspond to boulders initially emplaced in the LGM terminal moraines upstream

from the Xidatan–Dongdatan bajada. The fourth one (40.9 ka, site 3) could derive from an even older moraine of glacial stage 3 (Duplessy 1996; Thompson *et al.* 1997).

At a greater scale, the analysis of our SPOT image coverage makes it possible to test whether sinistral offsets along the fault between  $91^\circ\text{E}$  and  $102^\circ\text{E}$  are consistent with the climatically induced formation of landforms. This can be done by extrapolating our field results to stretches of the fault that we did not visit, over a length of nearly 1000 km. To first order, we simply assume that the fault, which exhibits between these longitudes one principal, fairly continuous strand, has slipped at a uniform and constant rate of  $12 \text{ mm yr}^{-1}$  during the last 600 000 yr. We then use the offsets of geomorphic markers to infer their age.

About 300 geomorphic offsets can be measured with reasonable accuracy on the panchromatic images (pixel size of 10 m; Table B5). Typical examples of such offsets along the Kusai Hu segment of the fault are shown in Fig. B3. The offsets mapped west of Kusai lake concern streams and fluvial terrace risers. They range between 25 and 110 m and can be reconstructed unambiguously, even for the smallest ones, whose size is close to the resolution of the images.

Fig. 32 displays all the offset values smaller than 5000 m listed in Table B5, together with their inferred ages, as a function of longitude along the fault. Note that offsets greater than 500 m are mostly observed in two rather restricted regions along the Kusai and Maqen segments of the fault. The reasons why such large offsets are preserved only in these two areas may be different. Near Kusai Hu, a relatively stable, long-term imprint of glacial action on the landscape may have been favoured by the permanence of a sizable ice-cap north of a very broad bajada draining into the interior of the high plateau. Near Maqen, it appears that deeper incision due to down-dropping of the regional base-level of the Huang He, which descends in steps towards the north, has forced the courses of its tributaries to remain captive to the surrounding relief (e.g. Gaudemer *et al.* 1989, 1995a; Replumaz *et al.* 2001).

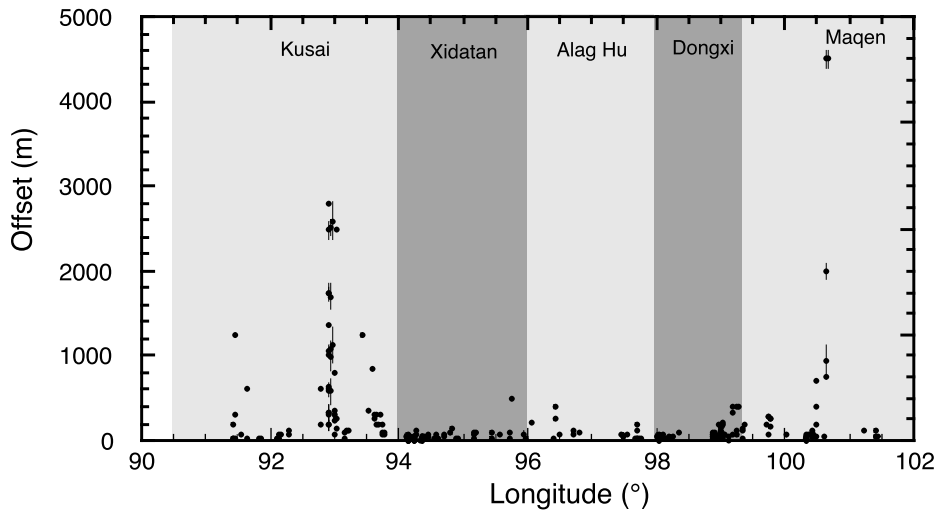


Figure 32. Geomorphic offsets measured on SPOT images plotted as a function of longitude along Kunlun Fault from west to east.

This notwithstanding, with the assumption made, most of the offsets preserved along the fault appear to post-date the LGM (Fig. 33). More specifically, ~70 per cent of the offsets are of Holocene age ( $\leq 10$  ka), and about 80 per cent are younger than 20 ka. More than 95 per cent of the offsets are younger than the penultimate (Riss) glacial maximum (~140 ka; Fig. 33).

Along the ~15 km long stretch of the Kunlun Fault near Kusai Hu, we have mapped the broadest spread of channel offsets, between 300 and 2.8 km (Figs 32 and 34). Most of them concern particularly broad, flat-floored valleys which appear to be of glacial origin, an inference corroborated by the facts that the fault lies here just south of a fairly large residual ice-sheet capping the Kunlun range (Fig. 34) and that the valleys incise widespread till with large boulders. Assuming a rate of  $12 \text{ mm yr}^{-1}$ , the most significant peaks in the offset distribution would have ages ranging between 4.5 and 230 ka (Fig. 35). The principal peaks would appear to correspond to the  $\delta^{18}\text{O}$  minima found by Thompson *et al.* (1997) in the Guliya

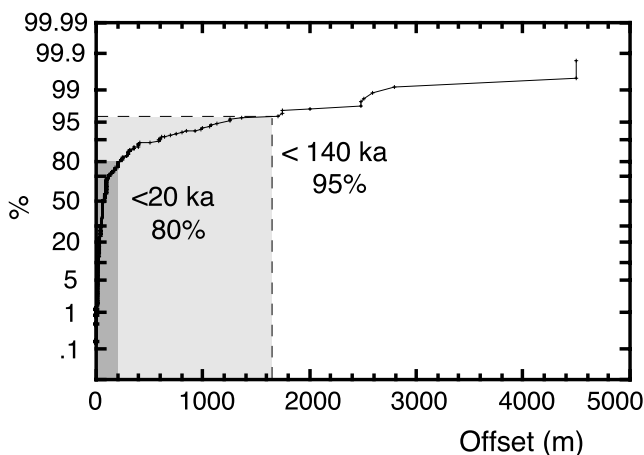


Figure 33. Percentage of offsets younger than 140 ka and 20 ka assuming a rate of  $12 \text{ mm yr}^{-1}$  along Kunlun Fault.

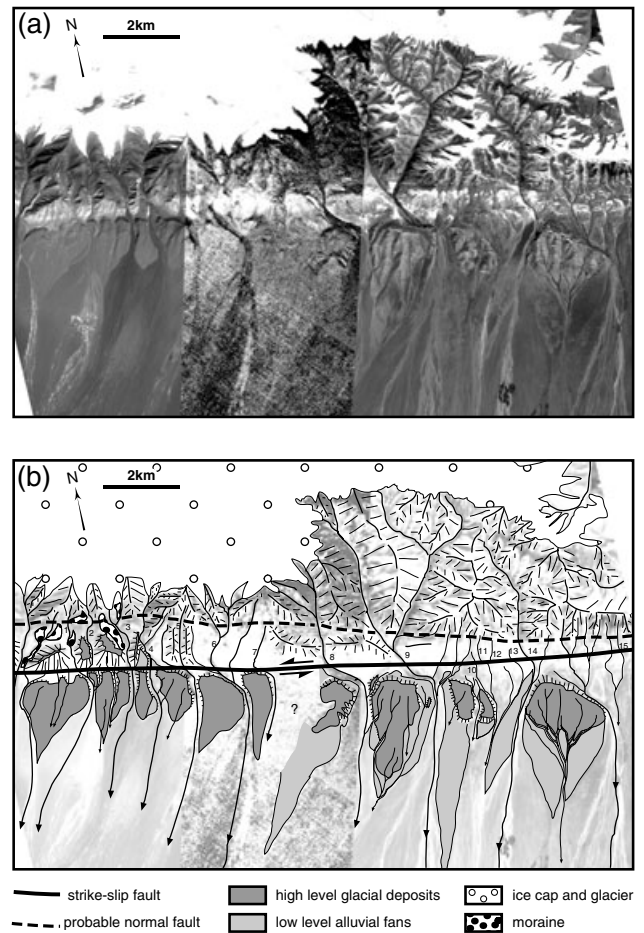
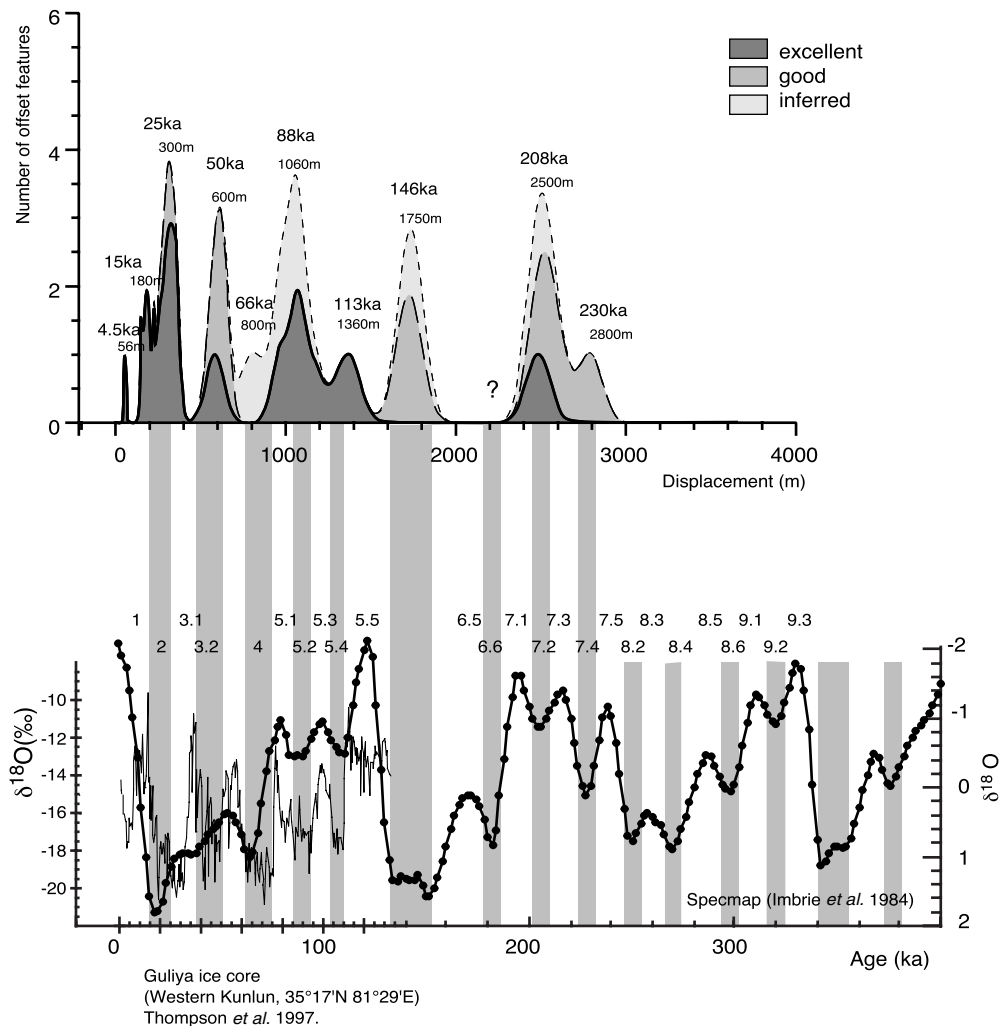


Figure 34. (a) Mosaic of Landsat and SPOT images KJ234-278 and KJ236-278 of a fault strand northeast of Kusai lake (see Fig. 2 for location). South of the ice-capped range, stream beds incised in Pleistocene morainic deposits are offset several hundred metres. (b) Schematic interpretation. Offsets of numbered streams are measured (see Table B4).



**Figure 35.** Summed Gaussian density probability function (top) of width  $\sigma$  for 31 offset measurements affected by error  $2\sigma$  along a 15 km long strand of Kunlun Fault north of Kusai lake shown in Fig. 34. Model ages calculated assuming a mean slip-rate of  $12 \text{ mm yr}^{-1}$  appear to correspond to cold glacials or stadials. The low  $\delta^{18}\text{O}$  values (below) measured in an ice core from western Tibet (Guliya ice cap, Thompson *et al.* 1997) and from the Specmap  $\delta^{18}\text{O}$  deep-sea core record (Imbrie *et al.* 1984) can be correlated with most offsets.

ice core of the Western Kunlun during the last 130 kyr, and to those of the Specmap deep-sea core record in the last 250 kyr (Imbrie *et al.* 1984; Fig. 35). Thus, at a more detailed level of correlation, this observation would support the inference that the main channels were incised into the south Kunlun bajada by glaciers that advanced farthest across the fault during the coldest climatic spells coeval with the  $\delta^{18}\text{O}$  minima. That the fault trace lies here only 2–5 km south of the edge of the present-day,  $\sim 6000$  m high ice cap is in keeping with this interpretation.

Hence, although one should be careful to take into account the different responses of glacial and fluvial landscapes to climatic forcing, both our field evidence, which rests firmly on accurate age determinations, and the inferences we deduce from simply extrapolating the rate we measure in the field to most of the fault length appear to support the idea that much of the geomorphic imprint visible on the northern Tibet plateau is punctuated by climatic events (e.g. Armijo *et al.* 1986, 1989; Gaudemer *et al.* 1995b; Peltzer *et al.* 1988b), particularly by the extreme differences in temperature and moisture that characterize glacial maxima and interglacials or stadials.

## 6 CONCLUSIONS

Our results imply that the Kunlun Fault has a constant slip-rate, of the order of  $12 \text{ mm yr}^{-1}$ , over a length of  $\sim 600$  km and a time-span of  $\sim 40\,000$  yr (Fig. 31). Whether other segments to the west and east of the sites we studied slip at precisely the same rate remains to be demonstrated. Fault morphology visible on SPOT images and the offset measurements derived from these images suggest that this may be the case. Beyond the western and eastern bounds of this study, more precisely west of  $90.5^\circ\text{E}$  and east of  $105^\circ\text{E}$ , the fault geometry changes, and left-lateral displacements may be distributed between the several fault strands that control slip transfer at the fault extremities. Our data support the inference that much of the present-day horizontal shear between Qaidam and Tibet is localized along the Kunlun Fault zone (Meyer *et al.* 1998; Fig. 1). Fairly fast slip along this narrow zone absorbs a significant fraction (1/3–1/2) of the eastward motion of Tibet relative to Siberia (e.g. Avouac & Tapponnier 1993; Peltzer & Saucier 1996).

The rate we determined and the minimum and multiple seismic offsets we measured suggest that, to first order, the seismic behaviour of the segments of the fault we studied in the field is characterized by fairly regular successions of large, similar earthquakes. For the two stretches of the fault where our data is most accurate, the recurrence times, characteristic slips and magnitudes of such earthquakes appear to be different. Characteristic events on the Dongxi Co segment of the Kunlun Fault seem to be smaller ( $M \sim 7.5$ ) and about twice as frequent ( $T_r \sim 420$  yr) than on the Xidatan–Dongdagan segment ( $M \sim 8$ ;  $T_r \sim 900$  yr).

By assuming a constant rate along most of the fault, we estimated the age of offset morphological markers elsewhere along segments that we could not reach in the field. Most of the depositional fluvial landforms appear to have been emplaced after the Last Glacial Maximum, during the wetter period of the Early Holocene optimum (Gasse *et al.* 1991) and the Late Holocene climate changes (Liu *et al.* 1998). Older features, like glacially carved or fluvial valleys, seem to be related to cold events of the last glacial stage.

That landform evolution was modulated by climate variability contradicts the view that the imprint of climate change on geomorphology cannot be used to infer ages of chief elements of the landscape, and hence orders of magnitude of slip-rates on active faults (e.g. Gillespie & Molnar 1995; Ritz *et al.* 1995). For this latter approach to be successful, however, a proper understanding of the regional geomorphic framework must first be obtained through careful analysis of landforms, which requires the combined use of satellite images, air photos and field evidence (e.g. Armijo *et al.* 1986, 1989; Avouac *et al.* 1993; Gaudemer *et al.* 1995b; Meyer *et al.* 1996; Peltzer *et al.* 1988b).

## ACKNOWLEDGMENTS

We thank the Institute of Geology of the Ministry of Land and Resources of China, in Beijing, the Institut National des Sciences de l'Univers (INSU, Paris, France), and the Institute of Geophysics and Planetary Physics at Lawrence Livermore National Laboratory (Livermore, USA) operating under the auspices of DOE contract W-7405-ENG48 for logistical and financial support. We are particularly indebted to Xu Zhiqin, Zhao Guoguang and Yang Jinshui for the excellent organization of the field logistics in China, and, on the French side, to G. Aubert and J. C. Rossignol for the launching and implementation of the East-Kunlun, French–Chinese cooperation project. The SPOT satellite images were acquired through the Tectoscope program, cosponsored by CNRS and INSU. We thank M. Kashgarian from the Center for Accelerator Mass Spectrometry at the Lawrence Livermore National Laboratory (Livermore, USA) for radiocarbon dating. We had stimulating discussions, either in the field or in the lab, with M. Brunel, U. Schärer, N. Arnaud, F. Gasse, J.P. Cogné, J. Marcoux, Chen Yan, J. Malavieille, He Qunlu, A. Assaraj. We are also grateful to both William Bull and Ray Weldon for fruitful comments on an earlier version of the manuscript. We thank R. Arrowsmith and an anonymous reviewer for their comments which helped improve the manuscript. This is IPGP contribution No. 1651 and LLNL contribution UCRL-JC-137203.

## SUPPLEMENTARY MATERIAL

Appendices A, B and C can be found online at <http://www.blackwell-science.com/products/journals/suppmat/GJI/GJI1556/GJI1556smA.htm>  
<http://www.blackwell-science.com/products/journals/suppmat/GJI/GJI1556/GJI1556smB.htm>  
<http://www.blackwell-science.com/products/journals/suppmat/GJI/GJI1556/GJI1556smC.htm>

## REFERENCES

- Anderson, R.S., Repka, J.L. & Dick, G.S., 1996. Explicit treatment of inheritance in dating depositional surfaces using in situ  $^{10}\text{Be}$  and  $^{26}\text{Al}$ , *Geology*, **24**, 47–51.
- Armijo, R., Tapponnier, P., Mercier, J.L. & Han, T.L., 1986. Quaternary extension in southern Tibet: field observations and tectonic implications, *J. geophys. Res.*, **91**, 13 803–13 872.
- Armijo, R., Tapponnier, P. & Han, T., 1989. Late Cenozoic right-lateral strike-slip faulting in southern Tibet, *J. geophys. Res.*, **94**, 2787–2838.
- Arnaud, N.O., Brunel, M., Roger, F., Shärer, U., Malavieille, J. & Tapponnier, P., 1997. Age, duration and thermal conditions associated with major strike-slip faults: examples from Northern Tibet, EUG9, *Abstract suppl.* **1**, *Terra Nova*.
- Assaraj, A., 1997. Changements hydroclimatiques depuis 13000 ans BP au Tibet Oriental et au nord du Xinjiang (Chine). Approche par l'étude de quelques enregistrements lacustres, *PhD thesis*, Université de Paris-Sud, Orsay.
- Avouac, J.P. & Tapponnier, P., 1993. Kinematic model of active deformation in Central Asia, *Geophys. Res. Lett.*, **20**, 895–898.
- Avouac, J.P., Tapponnier, P., Bai, M., You, H. & Wang, G., 1993. Active thrusting and folding along the northern Tien Shan and late Cenozoic rotation of the Tarim relative to Dzungaria and Kazakhstan, *J. geophys. Res.*, **98** (B4), 6655–6804.
- Bard, E., Hamelin, B., Fairbanks, R.G. & Zindler, A., 1990. Calibration of the  $^{14}\text{C}$  timescale over the past 30,000 years using mass spectrometric U-Th ages from Barbados corals, *Nature*, **345**, 405–410.
- Bierman, P.R., Gillespie, A.R. & Caffee, M.W., 1995. Cosmogenic ages for earthquake recurrence intervals and debris flow fan deposition, Owens Valley, California, *Science*, **270**, 447–450.
- Brown, E.T., Bourlès, D.L., Burchfiel, B.C., Deng, Q., Li, J., Molnar, P., Raisbeck, G.M. & You, F., 1998. Estimation of slip rates in the southern Tien Shan using cosmic ray exposure dates of abandoned alluvial fans, *Geol. Soc. Am. Bull.*, **110**, 377–386.
- Bull, W.B., 1991. *Geomorphic Responses to Climatic Change*, Oxford University Press, Oxford.
- Chang, C. *et al.*, 1986. Preliminary conclusions of the Royal Society and Academia Sinica 1985 geotraverse of Tibet, *Nature*, **323**, 501–507.
- Chen, S.F., Wilson, C.J.L., Dong, D.Q., Lin, Z.X. & Li, L.Z., 1994. Active faulting and block movement associated with large earthquakes in the Min Shan and Longmen Mountains, northeastern Tibetan Plateau, *J. geophys. Res.*, **99** (B12), 24 025–24 038.
- Chen, Z., Burchfiel, B.C., Liu, Y., King, R.W., Royden, L.H., Tang, W., Wang, E., Zhao, J. & Zhang, X., 2000. Global Positioning System measurements from eastern Tibet and their implications for India/Eurasia intercontinental deformation, *J. geophys. Res.*, **105**, 16 215–16 227.
- Coward, M.P., Kidd, W.S.F., Pan, Y., Shackleton, R.M. & Zhang, H., 1988. The structure of the 1985 Tibet Geotraverse, Lhasa to Golmud, *Phil. Trans. R. Soc. Lond.*, **327**, 307–336.
- Cui, Z. & Yang, B., 1979. On the Tuosuo-hu-Maqu active fault zone, *Northwest. seism. J.*, **1**, 57–61 (in Chinese).

- Defense Mapping Agency, 1980. *Operational Navigation Chart Series, Sheet G7*, DMA, St Louis, USA.
- Defense Mapping Agency, 1987. *Operational Navigation Chart Series, Sheet G8*, DMA, St Louis, USA.
- Defense Mapping Agency, 1988. *Operational Navigation Chart Series, Sheet G9*, DMA, St Louis, USA.
- Deng, Q., Song, F., Zhu, S., Li, M., Wang, T., Zhang, W., Burchfiel, B.C., Molnar, P. & Zhang, P., 1984. Active faulting and tectonics of the Ningxia-Hui autonomous region, *J. geophys. Res.*, **89**, 4427–4445.
- Deng, Q.S. *et al.*, 1986. Variations in the geometry and amount of slip on the Haiyuan (Nanxihaushan) fault zone, China, and the surface rupture of the 1920 Haiyuan earthquake, in *Earthquake Source Mechanics, Geophys. Monogr. Ser. Vol. 37*, pp. 169–182, eds Das, S., Boatwright, J. & Scholz, C., Am. Geophys. Un., Washington, DC.
- Derbyshire, E., 1987. A history of glacial stratigraphy in China, *Quat. Sci. Rev.*, **6**, 301–314.
- Derbyshire, E., Shi, Y., Li, J., Zheng, B., Li, S. & Wang, J., 1991. Quaternary glaciation of Tibet; the geological evidence, *Quat. Sci. Rev.*, **10**, 485–510.
- Duplessy, J.C., 1996. *Quand L'océan se Fâche, Histoire Naturelle du Climat*, ed. Odile Jacob, Paris.
- England, P.C. & Houseman, G., 1986. Finite strain calculations of continental deformation. 2. Comparison with the India-Asia collision zone, *J. geophys. Res.*, **91**, 3664–3676.
- England, P.C. & Molnar, P., 1990. Right-lateral shear and rotation as the explanation for strike-slip faulting in eastern Tibet, *Nature*, **344**, 140–142.
- England, P.C. & Molnar, P., 1997. Active deformation of Asia: From kinematics to dynamics, *Science*, **278**, 647–650.
- Gasse, F.M. *et al.*, 1991. A 13,000-year climate record from western Tibet, *Nature*, **353**, 742–745.
- Gaudemer, Y., Tapponnier, P. & Turcotte, D.L., 1989. River offsets across active strike-slip faults, *Ann. Tecton.*, **III** (2), 55–76.
- Gaudemer, Y., Tapponnier, P., Van Der Woerd, J. & Meyer, B., 1995a. Block rotations, fault bending and mountain building, EUG8, Abstract Suppl. 1, *Terra nova*, **7**.
- Gaudemer, Y., Tapponnier, P., Meyer, B., Peltzer, G., Guo, S.M., Chen, Z.T., Dai, H.G. & Cifuentes, I., 1995b. Partitioning of crustal slip between linked, active faults in the eastern qilian shan, and evidence for a major seismic gap, the 'Tianzhu gap', on the western haiyuan fault, Gansu (China), *Geophys. J. Int.*, **120**, 599–645.
- Ge, S., Bai, M., Li, Y., Liu, G., Zhen, Q., Zheng, J. & Zhu, S., 1992. *Active Altyn Tagh Fault Zone*, Seismological Press, Beijing.
- Gillespie, A. & Molnar, P., 1995. Asynchronous maximum advances of mountain and continental glaciers, *Rev. geophys.*, **33**, 311–364.
- Gu, G., Tinghuang, L. & Zhenliang, S., 1989. *Catalogue of Chinese Earthquakes (1831 BC–1969 AD)*, Science Press, Beijing.
- Hancock, G.S., Anderson, R.S., Chadwick, O.A. & Finkel, R.C., 1999. Dating fluvial terraces with <sup>10</sup>Be and <sup>26</sup>Al profiles: Application to the Wind River, Wyoming, *Geomorphology*, **27**, 1–2.
- Imbrie, J., Hays, J.D., Martinson, D.G., McIntyre, A., Mix, A.C., Morley, J.J., Pisias, N.G., Prell, W.L. & Shackleton, N.J., 1984. The orbital theory of the Pleistocene climate: support from a revised chronology of the marine d<sup>18</sup>O record, in *Milankovitch and Climate*, pp. 269–305, Dordrecht.
- Kidd, W.S.F. & Molnar, P., 1988. Quaternary and active faulting observed on the 1985 Academia Sinica–Royal Society geotraverse of Tibet, *Phil. Trans. R. Soc. Lond.*, **327**, 337–3363.
- Kirby, E., Whipple, K.X., Burchfiel, B.C., Wenqing Tang, Berger, G., Zhiming Sun, Zhiliang Chen, 2000. Neotectonics of the Min Shan, China: Implications for mechanisms driving Quaternary deformation along the eastern margin of the Tibetan Plateau, *Geol. Soc. Am. Bull.*, **112**, 375–393.
- Kohl, C.P. & Nishiizumi, K., 1992. Chemical isolation of quartz for measurement of in-situ produced cosmogenic nuclides, *Geochim. Cosmochim. Acta*, **56**, 3583–3587.
- Lal, D., 1991. Cosmic ray labeling of erosion surfaces: In situ production rates and erosion models, *Earth planet. Sci. Lett.*, **104**, 424–439.
- Lavé, J., 1997. Tectonique et érosion: l'apport de la dynamique fluviale à l'étude sismotectonique de l'Himalaya du Népal central, *PhD thesis*, Université Paris VII, Paris.
- Lehmkuhl, F., Owen, L.A. & Derbyshire, E., 1998. Late Quaternary glacial history of Northeast Tibet, *Quat. Proc.*, **6**, 121–142.
- Li, L. & Jia, Y., 1981. Characteristics of the deformation band of the 1937 Tuosuohe earthquake (M=7.5) in Qinghai, *Northwest. seism. J.*, **3**, 61–65.
- Li, J. *et al.*, 1997. Magnetostratigraphic dating of river terraces: rapid and intermittent incision of the Yellow River of the northeastern margin of the Tibetan Plateau during the Quaternary, *J. geophys. Res.*, **102**, 10 121–10 132.
- Lister, G.S., Kelts, K. & Chen, K., Yu, J. & Niessen, F., 1991. Lake Qinghai, China: closed-basin lake levels and the oxygen isotope record for ostracods since the latest Pleistocene, *Paleogeog., Paleoclimat., Paleoecol.*, **84**, 141–162.
- Liu, Q., 1993. Paléoclimat et contraintes chronologiques sur les mouvements récents dans l'ouest du Tibet: failles du Karakorum et de Longmu Co-Gosa Co, lacs en pull-apart de Longmu Co et de Sumxi Co, *PhD thesis*, Université Paris VII, Paris.
- Meyer, B., 1991. Mécanismes des grands tremblements de terre et du raccourcissement crustal oblique au bord nord-est du Tibet, *PhD thesis*, Université Paris VII, Paris.
- Meyer, B., Tapponnier, P., Gaudemer, Y., Peltzer, G., Guo, S.M. & Chen, Z.T., 1996. Rate of left-lateral movement along the easternmost segment of the Altyn Tagh fault, east of 96°E (China), *Geophys. J. Int.*, **124**, 29–44.
- Meyer, B., Tapponnier, P., Bourjot, L., Métivier, F., Gaudemer, Y., Peltzer, G., Shunmin, G. & Zhilai, C., 1998. Crustal thickening in Gansu-Qinghai, lithospheric mantle, and oblique, strike-slip controlled growth of the Tibet plateau, *Geophys. J. Int.*, **135**, 1–47.
- Mock, C., Arnaud, N.O. & Cantagrel, J.-M., 1999. An early unroofing in northeastern Tibet? Constraints from <sup>40</sup>Ar/<sup>39</sup>Ar thermochronology on granitoids from the eastern Kunlun range (Qinghai, NW China), *Earth planet. Sci. Lett.*, **171**, 107–122.
- Molnar, P. & Deng, Q., 1984. Faulting associated with large earthquakes and the average rate of deformation in central and eastern Asia, *J. geophys. Res.*, **89**, 6203–6227.
- Molnar, P. & Lyon-Caen, H., 1989. Fault plane solutions of earthquakes and active tectonics of the Tibetan Plateau and its margins, *Geophys. J. Int.*, **99**, 123–153.
- Molnar, P., Brown, E.T., Burchfiel, B.C., Qidong, D., Xianyue, F., Jun, L., Raisbeck, G.M., Jianbang, S., Zhangming, W., You, F. & Huichan, Y., 1994. Quaternary climate change and the formation of river terraces across growing anticlines on the north flank of the Tien Shan, China, *J. Geol.*, **102**, 583–602.
- Nishiizumi, K., Winterer, E.L., Kohl, C.P., Klein, J., Middleton, R., Lal, D. & Arnold, J.R., 1989. Cosmic ray production rates of <sup>10</sup>Be and <sup>26</sup>Al in quartz from glacially polished rocks, *J. geophys. Res.*, **94** (B12), 17 907–17 915.
- Pachur, H.-J., Wunnemann, B. & Zhang, H., 1995. Lake evolution in the Tengger Desert, Northwestern China, during the last 40,000 years, *Quat. Res.*, **44**, 171–180.
- Peltzer, G. & Saucier, F., 1996. Present-day kinematics of Asia derived from geologic fault rates, *J. geophys. Res.*, **101**, 27 943–27 956.
- Peltzer, G. & Tapponnier, P., 1988a. Formation and evolution of strike-slip faults, rifts, and basins during the India-Asia collision: an experimental approach, *J. geophys. Res.*, **93**, 15 095–15 117.
- Peltzer, G., Tapponnier, P., Gaudemer, Y., Meyer, B., Guo, S., Yin, K., Chen, Z. & Dai, H., 1988b. Offsets of late quaternary morphology, rate of slip, and recurrence of large earthquakes on the Chang Ma fault (Gansu, China), *J. geophys. Res.*, **93** (B7), 7793–7812.
- Peltzer, G., Tapponnier, P., Zhang, Z. & Xu, Z.Q., 1985. Neogene and Quaternary faulting in and along the Qinling Shan, *Nature*, **317**, 500–505.

- Peltzer, G., Crampé, F. & King, G., 1999. Evidence of nonlinear elasticity of the crust from the Mw 7.6 Manyi (Tibet) earthquake, *Science*, **286**, 272–276.
- Phillips, F.M., Zreda, M.G., Gosse, J.C., Klein, J., Evenson, E.B., Hall, R.D., Chadwick, O.A. & Sharma, P., 1997. Cosmogenic  $^{36}\text{Cl}$  and  $^{10}\text{Be}$  of Quaternary glacial and fluvial deposits of the Wind River Range, Wyoming, *Geol. Soc. Am. Bull.*, **109**, 1453–1463.
- Qian, F., Ma, X., Wu, X. & Pu, Q., 1982. Study of the magnetic stratigraphy of the Qiantang and Quguo formations, in *Contributions to the Geology of the Qinghai-Xizang (Tibet) Plateau*, **4**, 121–130 (in Chinese).
- Repka, J.L., Anderson, R.S. & Finkel, R.C., 1997. Cosmogenic dating of fluvial terraces, Fremont River, Utah, *Earth planet. Sci. Lett.*, **152**, 59–73.
- Replumaz, A., Lacassin, R., Tapponnier, P. & Leloup, P.H., 2001. Large river offsets and Plio-Quaternary dextral slip rate on the Red River Fault (Yunnan, China), *J. geophys. Res.*, **106**, 819–836.
- Ritz, J.F., Brown, E.T., Bourlès, D.L., Philip, H., Schlupp, A., Raisbeck, G.M., Yiou, F. & Enkhtuvshin, B., 1995. Slip-rates along active faults estimated with cosmic-ray-exposure dates: application to the Bogd Fault, Gobi-Altai, Mongolia, *Geology*, **23**, 1019–1022.
- Siame, L.L., Bourlès, D.L., Sébrier, M., Bellier, O., Castano, J.C., Araujo, M., Perez, M., Raisbeck, G.M. & You, F., 1997. Cosmogenic dating ranging from 20 to 700 ka of a series of alluvial fan surfaces affected by the El Tigre fault, Argentina, *Geology*, **25**, 975–978.
- Sieh, K.E. & Jahns, R.H., 1984. Holocene activity of the San Andreas fault at Wallace Creek, California, *Geol. Soc. Am. Bull.*, **95**, 883–896.
- Tapponnier, P. & Molnar, P., 1977. Active faulting and tectonics in China, *J. geophys. Res.*, **82**, 2905–2930.
- Tapponnier, P., Peltzer, G., Le Dain, A.Y., Armijo, R. & Cobbold, P., 1982. Propagating extrusion tectonics in Asia: New insights from simple experiments with plasticine, *Geology*, **10**, 611–616.
- Tapponnier, P., Meyer, B., Avouac, J.P., Peltzer, G., Gaudemer, Y., Guo, S., Xiang, H., Yin, K., Chen, Z., Cai, S. & Dai, H., 1990. Active thrusting and folding in the Qilian Shan, and decoupling between upper crust and mantle in northeastern Tibet, *Earth planet. Sci. Lett.*, **97**, 382–403.
- Thompson, L.G., Mosley-Thompson, E., Davis, M.E., Bolzan, J.F., Dai, J., Yao, T., Gundestrup, N., Wu, X., Klein, L. & Xie, Z., 1989. Holocene–Late Pleistocene climatic ice core records from Qinghai-Tibetan Plateau, *Science*, **246**, 474–477.
- Thompson, L.G., Yao, T., Davis, M.E., Henderson, K.A., Mosley-Thompson, E., Lin, P.-N., Beer, J., Synal, H.-A., Cole-Dai, J. & Bolzan, J.F., 1997. Tropical climate instability: the last glacial cycle from a Qinghai-Tibetan ice core, *Science*, **276**, 1821–1825.
- Van Der Woerd, J., 1998. Couplage cinématique entre décrochements et chevauchements actifs dans le Nord du Tibet. Croissance du plateau Tibétain, *PhD thesis*, Université Paris VII-Denis Diderot, Paris.
- Van Der Woerd, J., Ryerson, F.J., Tapponnier, P., Gaudemer, Y., Finkel, R., Mériaux, A.S., Caffee, M., Guoguang, Z. & Qunlu, H., 1998. Holocene left slip-rate determined by cosmogenic surface dating on the Xidatan segment of the Kunlun fault (Qinghai, China), *Geology*, **26**, 695–698.
- Velasco, A.A., Amon, C.J. & Beck, S., 2000. Broadband source modeling of the November 8, 1997 Tibet, ( $M_w=7.5$ ) earthquake and its tectonic implications, *J. geophys. Res.*, **105**, 28 065–28 080.
- Wang, J. & Derbyshire, E., 1987. Climatic geomorphology of the North-Eastern part of the Qinghai-Xizang plateau, People's Republic of China, *Geograph. J.*, **153**, 59–71.
- Wang, Y.F., Wang, S.M., Xue, B., Ji, L., Wu, J.L., Xia, W.L., Pan, H.X., Zhang, P.Z. & Chen, F.H., 1995. Sedimentological evidence of the piracy of fossil Zoige Lake by the Yellow River, *Chin. Sci. Bull.*, **40**, 1539–1544.
- Weldon, R.J., 1986. Late cenozoic geology of Cajon Pass; implications for tectonics and sedimentation along the San Andreas fault, *PhD thesis*, California Institute of Technology, Pasadena.
- Weldon, R.J. & Sieh, K.E., 1985. Holocene rate of slip and tentative recurrence interval for large earthquakes on the San Andreas fault in Cajon Pass, southern California, *Geol. Soc. Am. Bull.*, **96**, 793–812.
- Wu, X., Qian, F. & Pu, Q., 1982. Quaternary glaciogeology of the east Kunlun mountains (in Chinese), in *Contributions to the Geology of the Qinghai-Xizang (Tibet) Plateau*, **4**, 1–18 (in Chinese).
- Yan, G., Wang, F.B., Shi, G.R. & Li, S.F., 1999. Palynological and stable isotopic study of palaeoenvironmental changes on the northeastern Tibetan plateau in the last 30,000 years, *Palaeogeogr. Palaeoclimat. Palaeoecol.*, **153**, 147–159.
- Zhang, B., Jiao, D., Zhang, P.P., Molnar, B.C., Burchfiel, D., Deng, Q., Wang, Y. & Song, F., 1987. Displacement along the Haiyuan fault associated with the great 1920 Haiyuan, China, earthquake, *Bull. seism. Soc. Am.*, **77**, 117–131.
- Zhang, Y.Q., Vergely, P. & Mercier, J., 1995. Active faulting in and along the Qinling range (China) inferred from SPOT imagery analysis and extrusion tectonics of South China, *Tectonophysics*, **243**, 69–95.
- Zhao, G., 1996. Quaternary faulting in north Qinghai-Tibet plateau, *Continental Dynamics, Beijing*, **1**, 30–37.
- Zhao, G., He, Q., Tapponnier, P. & Gaudemer, Y., 1994. Preliminary investigation on the Holocene paleoearthquake features along the mid-section of the Ku-ma active fault, East Kunlun, *Proc. First Symp. Geology and Geophysics of East Kunlun and its Adjacent Areas, Continental Geodynamics, Beijing, China*.